

# 1 Oblique rifting triggered by slab tearing : the case of the Alboran 2 rifted margin in the eastern Betics 3

4 Marine Larrey<sup>1,2</sup>, Frédéric Mouthereau<sup>1\*</sup>, Damien Do Couto<sup>3</sup>, Emmanuel Masini<sup>4</sup>, Anthony  
5 Jourdon<sup>5</sup>, Sylvain Calassou<sup>2</sup> and Véronique Mieggebielle<sup>2</sup>

6 <sup>1</sup>Université Paul Sabatier, Géosciences Environnement Toulouse, GET UMR 5563, Toulouse, France.

7 <sup>2</sup>TOTAL S.A., Centre Scientifique & Technique Jean Féger, Pau, France.

8 <sup>3</sup>Sorbonne Université, CNRS-INSU, Institut des Sciences de la Terre Paris, ISTeP UMR 7193, F-75005 Paris,  
9 France.

10 <sup>4</sup>M&U sas, France.

11 <sup>5</sup>Institute of Geophysics, Ludwig-Maximilians-Universität München, Munich, Germany.

12 *Corresponding author:* Frédéric Mouthereau (frederic.mouthereau@get.omp.eu)

13

## 14 Abstract

15 The tectonic evolution of highly oblique continental margins that result from extension above lithospheric STEP faults  
16 is poorly understood. Here, we investigate the case of the Alboran margin in the eastern Betics characterized by crustal  
17 thinning of 15-10 km, oblique to the direction of slab retreat. The current deformation patterns indicate that oblique  
18 rifting is underway. However, it is unclear whether these conditions are those that prevailed during the formation of  
19 the metamorphic domes and intramontane basins. We review the temporal and spatial evolution of Neogene  
20 sedimentary basins and brittle deformation in the eastern Betics, and exploit offshore seismic reflection lines to  
21 propose a crustal-scale section across the oblique margin. The history of sediment infill and rates of subsidence  
22 combined with the analyses of fault slip data, confirm that brittle extension oriented from N20°E to EW occurred  
23 during an interval spanning from the Serravallian-early Tortonian to the late Tortonian (14-8 Ma). This extension is  
24 associated with both normal and strike-slip regimes and the evolution of the strike-slip fault zones flanking the  
25 metamorphic domes. The transtensional model forms a coherent scheme linking the ductile deformation associated  
26 with metamorphic domes and the formation of EW- and NW-SE/NNW-SSE-directed sedimentary basins in the brittle  
27 upper crust during the Tortonian. The oblique extension, which is closely associated with STEP faulting, occurred  
28 during the regional convergence between Africa and Iberia since the Miocene. Only recently, around 8 Ma, slab  
29 detachment started to migrate westward, leading to tectonic inversion in the eastern Betics. Such a type of narrow  
30 oblique rifted margin associated with transform-like plate boundaries is not unique but is expected to be hardly  
31 preserved in the geological record due to the transient nature of retreating subduction systems.

Deleted: back-arc

Deleted: back-arc

Deleted: confirms

## 35 1 Tear faulting and the formation of oblique rifted margin in the Betics

36 Lithospheric tear faults or subduction-transform edge propagator (STEP) faults are propagating strike-slip faults that  
37 accommodate the differential motion between the retreating subduction zone and the overriding plate (Govers and  
38 Wortel, 2005). Because of the relative motion between back-arc and surrounding plates, they are also propagating  
39 strike-slip faults defined by a sharp contrast in crustal thickness. As noted by Govers and Wortel (2005) such oblique  
40 fault boundaries do not necessarily form proper transform plate boundaries but broad zones of distributed deformation,  
41 accommodating differential trench-parallel extension, strike-slip motion and rotation. In case the lithospheric tear  
42 propagates within the continent-ocean transition, a narrow continental margin forms highly oblique to the direction of  
43 back-arc extension. This is documented, for instance, in the Carribean, along the transcurrent Carribean-South  
44 America plate boundary (Pindell and Kennan, 2009) or on the margin of the South Orckney microcontinent, along the  
45 Scotia-Antarctic plate boundary (Dalziel et al., 2013). Despite the large-scale kinematic picture is relatively well  
46 understood, there are only few places on Earth where continental crustal deformation associated with slab-edge  
47 continental rift system can be studied both onland and offshore.

48 Here, we focus on the eastern Betic Cordillera, which constitutes a rifted margin defined by decreasing crustal  
49 thickness from >35 km to 20 km onshore (Diaz et al., 2016), thinning offshore to 16-6 km in the Eastern Alboran arc  
50 to back-arc region (Booth-Rea et al., 2018; Gómez de la Peña, 2020a) (Figs 1 and 2). This region is seen to develop  
51 above a EW-trending STEP fault at the boundary between the Alboran basin and the Iberian paleomargin (Badji et  
52 al., 2014; Gallais et al., 2013; Jolivet et al., 2021a; Mancilla et al., 2015a). The tectonic expression of the strike-slip  
53 deformation during E-W-directed crustal extension above the lithospheric tear is however controversial. On the one  
54 hand, low-angle ductile extensional detachments with a top-to-the-west sense of shear are the main features  
55 accommodating deformation in the overriding plate. Yet, a-type metamorphic domes in the lower crust, elongated  
56 parallel to the E-W direction (Fig. 1), formed during the early Miocene, are viewed to express the transtensional  
57 deformation at the tip of propagating tear (Pourhiet et al., 2012). On the other hand, E-W-directed transfer strike-slip  
58 faulting is interpreted as a late (post-middle Miocene) brittle deformation feature associated with differential E-W  
59 crustal extension between the metamorphic domes in the eastern Betics (Alpujarras fault zone ; Sanz de Galdeano and  
60 Vera, 1992; Sanz de Galdeano et al., 1985; Martínez-Martínez et al., 2006) and in the western Betics (Torcal fault  
61 zone ; Barcos et al., 2015) unrelated to ductile deformation (Fig. 1). In line with the latter interpretation, the dextral  
62 motion these transfer faults accommodate is assumed to be modest, reflecting a recent post-8 Ma kinematic change  
63 that accompanies the stalling of westward slab rollback, the onset of tectonic inversion in the Gibraltar Arc (Do Couto  
64 et al., 2014; d'Acromont et al., 2020; Jolivet et al., 2021a; Martínez-García et al., 2017), and progressive slab tearing  
65 and delamination of the lithospheric mantle from the eastern to the central Betics (Martínez-Martínez et al., 2006 ;  
66 Mancilla et al., 2015a ; García-Castellanos and Villaseñor, 2011; Spakman et al., 2018). Note that in a recent study  
67 the dextral displacement since 9 Ma has been estimated to more than 100 km along the Torcal fault (Crespo-Blanc et  
68 al., 2016).

69 The lack of structural, temporal constraints and quantification of belt-parallel motion along these faults indicates,  
70 however, that we do not yet fully understand their link with the long-term evolution of slab tearing and margin  
71 formation. For instance, the current deformation patterns in the Central Betics, where metamorphic domes are present,

Deleted: back-arc

Formatted: Font colour: Auto, English (US)

Deleted: transcurrent

Deleted: 1),

Deleted: e.g.

Deleted: Frasca

Deleted: 2016 ;

Formatted: English (US)

Deleted: strike-slip

Formatted: Font colour: Auto

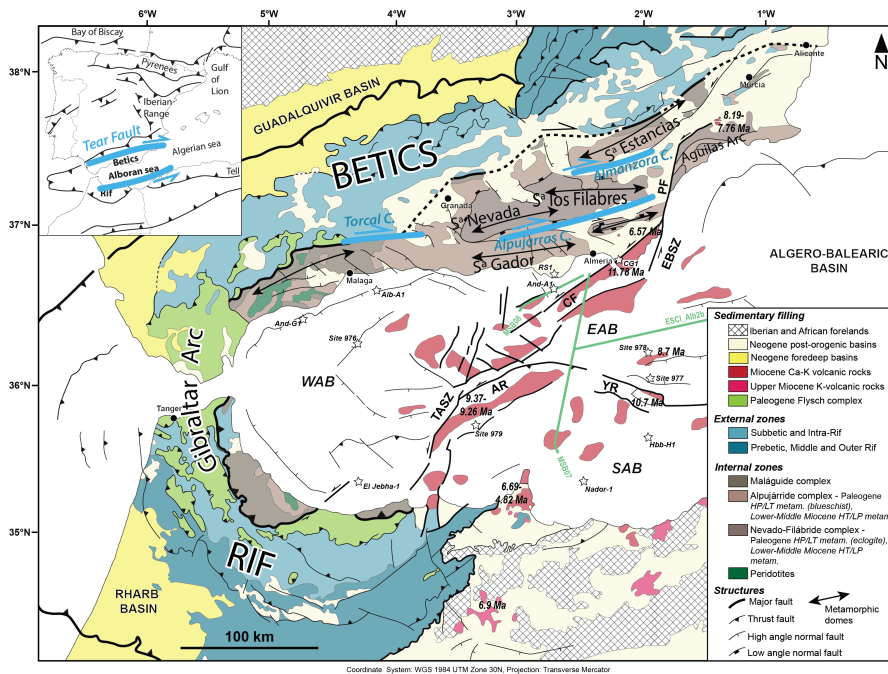
Deleted: →

80 brings evidence that both strike-slip faulting and extension operate synchronously (Martínez-Martínez et al., 2006).  
81 This is shown by the west-directed GPS velocities increasing westwards indicating ongoing extension, and the west-  
82 directed displacements increasing from North to South, towards the Alboran domain, revealing right-lateral shear (Fig.  
83 2). This together with evidence for present-day 4.5 mm/yr westward displacement and rotations in the Western Betics  
84 and Rif reveal that the westward slab rollback is likely to be still ongoing (Fadil et al., 2006; Gonzalez-Castillo et al.,  
85 2015). The current transtensional deformation across the Betic Cordillera is consistent with the current stress regime  
86 defined by extension direction highly oblique (max. 20°) to the Betic structural trend (or 70° spanned by the direction  
87 of extension and normal of the rift trend). Right-lateral transtensional deformation further agrees with the extrusion  
88 model of the Alboran basin towards the Gibraltar arc to the West (Borque et al., 2019; Palano et al., 2015) as a  
89 consequence of indentation by the east Alboran domain likely enhanced by resistance slab dragging (Spakman et al.,  
90 2018). In the East, the extrusion is accommodated by left-lateral strike-slip displacement along the Eastern Betic Shear  
91 Zone (EBSZ; Borque et al., 2019), shaped by the Carboneras Fault (CF) and Palomares Fault (PF), which separates  
92 the extrusion domain where extension and transtension is prevailing from the Águilas Arc where N-S indentation is  
93 well documented (Ercilla et al., 2022). In this region, This fault extends offshore, across the Alboran Sea, in the larger  
94 Trans-Alboran Shear Zone (De Larouzière et al., 1988; Stich et al., 2006) moving at ~4 mm/yr, equivalent to the  
95 regional 5 mm/yr NW-directed convergence between Africa (Nubia) and Europe (Fig. 2; Echeverría et al., 2013;  
96 Koulali et al., 2011; Nocquet, 2012; Palano et al., 2015, 2013; Vernant et al., 2010). Here, we hypothesize that the  
97 present-day oblique extension patterns is at play since the Miocene and explain the formation of the narrow Alboran  
98 rifted margin.  
99

Deleted: .

Deleted: The current transtensional

Formatted: English (US)

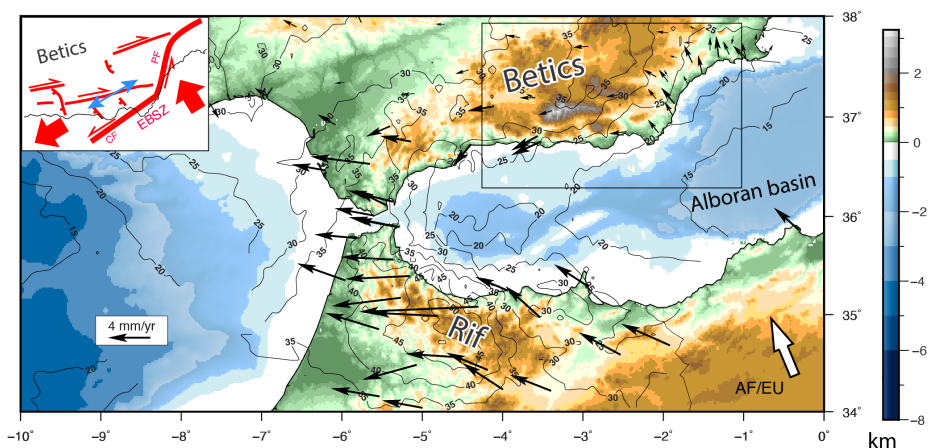


102  
 103 **Figure 1** : Geological map of the Betic-Rif arc. Main tectonic units and age of volcanism as well as major structures  
 104 and Neogene sedimentary basins are shown. The studied offshore seismic lines (red) is displayed as well as offshore  
 105 wells and ODP sites (★) for stratigraphic calibration in the East (EAB), South (SAB) and West Alboran basins  
 106 (WAB). CF: Carboneras Fault; PF: Palomares Fault; AR: Alboran Ridge; YR: Yusuf Ridge; EBSZ : East Betic Shear  
 107 Zone; TAsZ: Trans-Alboran Shear Zone.  
 108

109 Only recently high-resolution 3D numerical models have been able to predict the deep structure of oblique rift  
 110 domains. These models can be used as a guide to re-evaluate the evolution of the Betics. 3D models by Jourdon et al.  
 111 (2021) predict that oblique extension results in narrow rifted margins, strike-slip faults and corridors coupled with  
 112 subsident pull-apart basins, normal faults and block rotations (**Fig. 3**). The recognition of block rotation in the Betic  
 113 arc (Crespo-Blanc et al., 2016; Platzman, 1992), strike-slip fault zones (**Fig. 1**) and NW-SE normal faulting, which  
 114 defines extension direction highly oblique to the margin (Galindo-Zaldivar et al., 2003; **Figs 1 and 2**), support this  
 115 view. The simulations also show that the deeper ductile crust experiences thinning (vertical flattening) and stretching  
 116 perpendicular to the strike of the margin in accordance with stretching lineations parallel to the metamorphic domes  
 117 and low-angle detachments (**Fig. 3**). Other types of 3D numerical experiments show that sediment loading of strike-

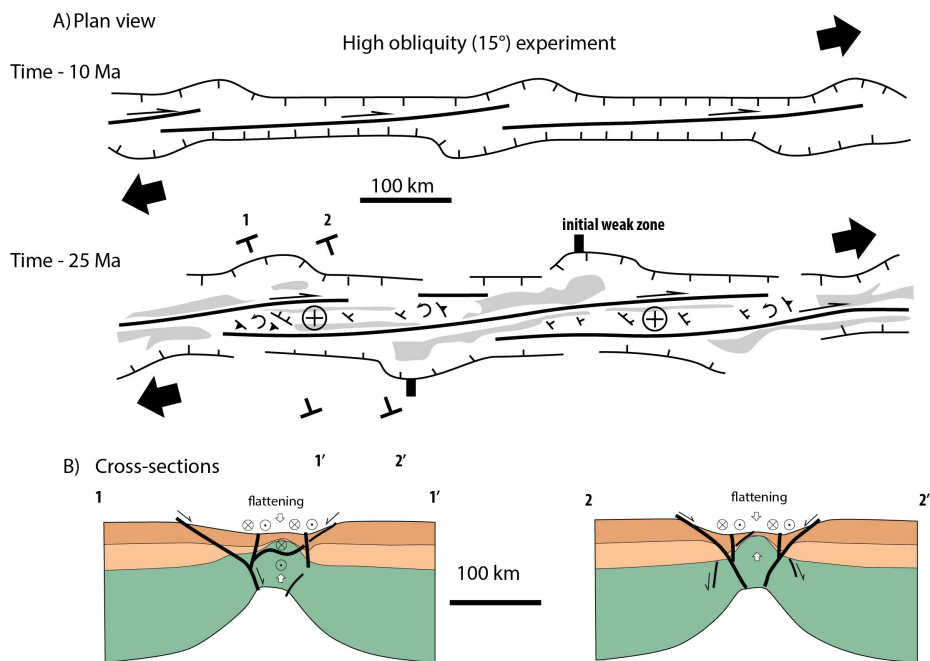


118 slip faults can result in asymmetric flexural basin with apparent normal fault throw (Neuharth et al., 2021) that can be  
 119 mistakenly interpreted as resulting from orthogonal extension. Asymmetric basins are indeed intriguing characteristics  
 120 of intramontane basins in the Betics (Rodríguez-Fernández et al., 2011; Augier et al., 2013; Do Couto et al., 2014 ;  
 121 Giaconia et al., 2014). Although primarily found associated with divergent plate boundaries e.g. in the Gulf of  
 122 California (Fossen et al., 2013; Fossen and Tikoff, 1998) highly oblique extension is also documented in active  
 123 transform regions along the San Andreas Fault (Teyssier and Tikoff, 1998) or the North Anatolian Fault in Marmara  
 124 Sea (Okay et al., 2004). A detailed analysis of highly oblique rifting deformation in the Gulf of California recognises  
 125 similar tectonic elements as for the Betics, such as extensional detachment systems orthogonal to the divergence and  
 126 upper crustal folds trending parallel to the divergence (Fossen et al., 2013).



127 **Figure 2** : Present-day kinematics in the Betic-Rif arc and eastern Betic Cordillera (inset). GNSS-based displacements  
 128 in the western Alboran block and north-western Africa shown in a fixed Eurasian reference frame (black arrows after  
 129 Palano et al., 2015) are oblique to the AF/EU plate convergence (white arrow) inferred from plate tectonic Morvel  
 130 model (Argus et al., 2011). Labelled contours depict the crustal depth given in kilometers as inferred from deep seismic  
 131 profiles and receiver functions analysis (Diaz et al., 2016). In the eastern Betic (inset), W-directed stretching is taken  
 132 up by EW-directed right-lateral strike-slip fault and NW-SE normal faults. Extension direction resolved from focal  
 133 mechanisms (blue arrows) are after (Stich et al., 2006). CF: Carboneras Fault; PF : Palomares Fault; AR: Alboran  
 134 Ridge; YR: Yusuf Ridge; EBSZ : East Betic Shear Zone; TASZ: Trans-Alboran Shear Zone.  
 135  
 136

137 Several tectonic features need further discussion however. First, the relevance of strike-slip faulting in the past is  
 138 debatable as only a few occurrence of crustal-scale strike-slip faults are mapped. Second, the detail of the temporal  
 139 and spatial relationships between the formation of the oblique/transform margin and STEP faulting remain elusive.  
 140 We here review the temporal and spatial evolution of Neogene intramontane sedimentary basins and related brittle  
 141 deformation in the eastern Betics. In addition, we exploit offshore seismic reflection lines to propose a new crustal-  
 142 scale section across the oblique margin. Based on these constraints we present a tectonic scenario for the formation of  
 143 the high-obliquity rifted margin controlled by STEP faulting.  
 144



145

146

147

148

149

150

151

152

153

**Figure 3** : Sketch showing two steps (after 10 Myrs and 24 Myrs) of a 3D thermo-mechanical model of oblique rifting in plan view (A) and cross-sections (B). Results are redrawn after (Jourdon et al., 2021) for the case of a highly oblique experiment where extension is set with an angle of 15° with respect to the rift axis. Grey regions in (A) are basins adjacent to uplifted domains (cross-circle symbol) associated with right-lateral strike-slip faults. Cross-sections (B) depict the abrupt crustal thinning that occur perpendicular. Crustal thinning is most visible for the lower crust and produces the formation of an abrupt necking domain controlled by rift-parallel normal faults dipping towards the center of the rift and right-lateral strike-slip faults.

154

## 2. Geodynamics and STEP faulting in the Betics

155

156

157

158

159

160

161

162

163

164

165

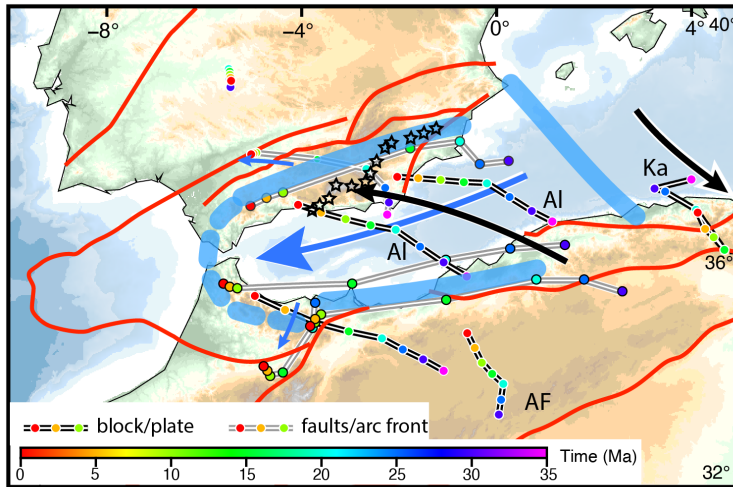
The onset of N-directed movement of Africa, by the Late Cretaceous-Paleogene, led to far-field, Laramide-like contraction from Morocco throughout Western Europe (Mouthereau et al., 2021). South of Iberia, in the Betic-Rif domain, the closure of hyper-extended rift systems and oceanic basins of the Atlantic-Alpine Tethys resulted in the development of a proto-Betic accretionary prism, likely largely submerged (Angrand and Mouthereau, 2021; Daudet et al., 2020; Vergés and Fernández, 2012). By about 50 Ma, the acceleration of plate convergence led to the shortening of continental rift and oceanic basins and topographic uplift all over Iberia (Daudet et al., 2020; Mouthereau et al., 2021, 2014; Rat et al., 2019; Vacherat et al., 2016; Waldner et al., 2021) associated with onset of continental rifting along the Western European Rift (e.g. Mouthereau et al., 2021). 35 Ma ago, as Africa convergence slowed down, the western Mediterranean sea opened accompanied by retreating slabs (Dewey, 1988; Dewey et al., 1989; Faccenna et al., 2014; Jolivet and Faccenna, 2000; Rosenbaum et al., 2002). Subduction occurred mainly before 30 Ma as argued by age constraints on high-pressure mineral assemblages (Augier et al., 2005a; Bessièrè et al., 2021; Booth-Rea et al.,

166 2015; Gomez-Pugnaire and Fernandez-Soler, 1987; Platt and Vissers, 1989; Platt and Whitehouse, 1999) and has been  
167 suggested to last until the mid-Miocene in the eastern Betics e.g. (Platt et al., 2013). The timing of formation of the  
168 Alboran basin is constrained to 23 to 16 Ma by the oldest deposits found on Alboran basement and by the timing of  
169 high-temperature metamorphic overprint and rapid cooling to shallow crustal temperature (Bessi re et al., 2021;  
170 Daudet et al., 2020; Janowski et al., 2017; Johnson et al., 1997; Platt et al., 2005; Sosson et al., 1998; V zquez et al.,  
171 2011; Zeck et al., 1992). The eastern Alboran basin formed later, mostly by late Miocene arc magmatism (Booth-Rea  
172 et al., 2007; 2018; G mez de la Pe a et al., 2020a).

173 All kinematic reconstructions agree that extension results from the westward migration of the arc front and retreat of  
174 the Alboran slab, well imaged below the Gibraltar arc as a steeply-dipping high-velocity anomaly (Bezada et al., 2013;  
175 Heit et al., 2017; Mancilla et al., 2018, 2015a, 2015b; Palomeras et al., 2014; Spakman and Wortel, 2004; Villase or  
176 et al., 2015). These reconstructions, however, differ according to the paleo-position of Alboran terrane, and hence to  
177 the amount and vergence of subduction (Angrand and Mouthereau, 2021; Hinsbergen et al., 2014; Lonergan and  
178 White, 1997; Romagny et al., 2020; Rosenbaum et al., 2002; Verg s and Fern ndez, 2012). Seismic tomography  
179 reveals that slab detachment and tearing occur along the conjugate Alboran margins of the southern Betics and  
180 northern Africa (Govers and Wortel, 2005; Heit et al., 2017; Mancilla et al., 2015a; Meighan et al., 2013; Spakman  
181 and Wortel, 2004).

182 In **Fig. 4** we refer to the reconstruction of Angrand and Mouthereau (2021) that has the advantage of reconciling  
183 previous western Mediterranean models (Romagny et al., 2020; Verg s & Fern ndez, 2012) with recent  
184 thermochronological analyses in western Betics (Daudet et al., 2020) and other geological data (see compilation in  
185 Mouthereau et al., 2021). This model considers that the Alboran domain has been rifted from Iberia during the Jurassic.  
186 It is in agreement with detrital and igneous zircon U-Pb ages that suggest Alboran was attached to Iberia in the late  
187 Paleozoic (Jabaloy-S nchez et al., 2021). It also accounts for the existence of an upper Cretaceous-Paleogene foreland  
188 basin that formed adjacent to a proto-Betic orogen and in continuity eastwards with the Balearic Promontory. In that  
189 respect, it contrasts with other models placing the Alboran domain to the south of the Balearic Promontory (Moragues  
190 et al., 2021; van Hinsbergen et al., 2014).

191 In this reconstruction about 400 km of slab retreat is estimated since about 35 Ma (gray path, blue arrows in **Fig. 4**).  
192 It is worth noting that for Romagny et al. (2020) a similar amount (i.e. 400 km) is accommodated by back-arc extension  
193 of the Alboran crust, implying the same magnitude of displacement along the STEP fault in the Betics. In the  
194 reconstruction of Angrand and Mouthereau (2021), however, crustal thinning in Alboran basin is linked to  
195 delamination retreat of the Alboran lithospheric mantle towards the west. Because of the decoupling between crust  
196 and mantle, the length of the delaminated slab resolved at depth in seismic tomography, should not be simply translated  
197 into the amount of E-W crustal extension in the Alboran domain. This further implies that the displacement across the  
198 STEP fault must be also less than 400 km. Daudet et al. (2020) suggested that an extension of 110 km estimated from  
199 the restoration of low-angle detachment systems in the central and eastern Betics (Martinez-Martinez et al., 2002) is  
200 likely to be a more accurate crustal estimate of the movement Alboran domain rather than the total slab length.  
201



202  
203  
204  
205  
206  
207  
208  
209  
210  
211

**Figure 4:** Kinematics of African plate (AF), Alboran (Al) and Kabyliides (Ka) blocks with respect to fixed European plate since 35 Ma reconstructed after Angrand and Mouthereau (2021). Thick blue lines depicts the approximate position of lithospheric tear faults (between Al and Europe and Africa) and transfer faults (between Al and Ka). Tear faults located in Betics and Rif are after Jolivet et al. (2021b). Black stars depicts the positioned of tear fault in the Betics as defined by Mancilla et al. (2015a). Black arrows indicate the movement of Al and Ka with respect to Europe along black motion paths presented from 35 Ma to present. Grey motion paths refer to the motion of specific structures relative to Europe, including the motion of the arc front (thick blue dashed line) and faults in red. Dark blue arrow depicts the movement of the arc front due to retreating delamination towards the west.

212 **3. Miocene extension in the eastern Betics**

213 **3.1 Relationships between domes and basins : from transtension and pure extension to late tectonic inversion**

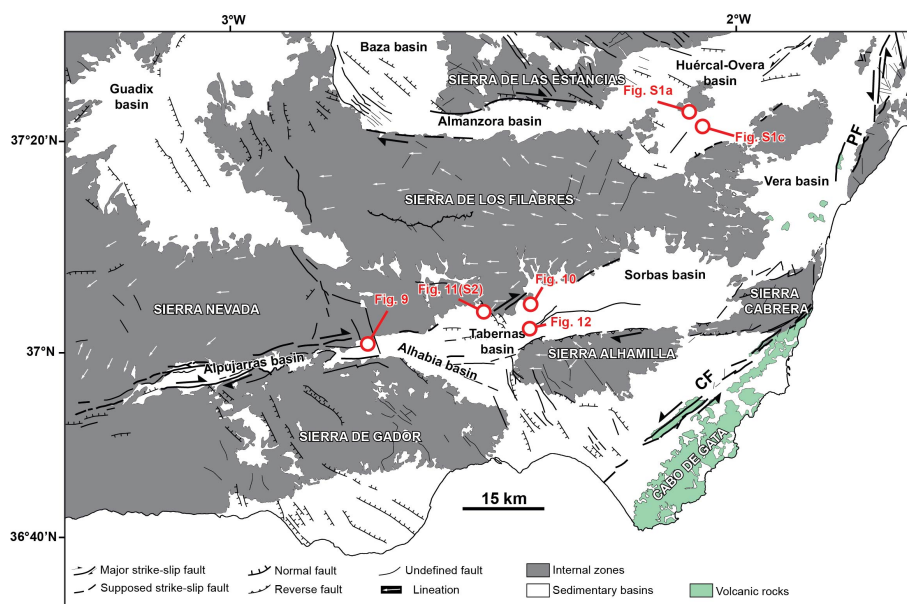
214 The most prominent extensional features in the eastern Betics are : 1) E-W elongated ranges that formed metamorphic  
215 domes with foliations bearing prominent E-W stretching lineations, for instance, in the Nevado-Filabrides  
216 Complex (Fig. 5; e.g. Sierra de los Filabres, Sierra Nevada, and the Sierra de las Estancias) and Serravallian-Tortonian  
217 sedimentary basins (Tabernas-Sorbas, Alpujarras, Almanzora and Huércal-Overa basins); 2) NNW-SSE/NW-SE  
218 normal fault systems and basins oblique to the domes such as the NW-SE trending Guadix-Baza and Alhabia basins  
219 (Galindo-Zaldivar et al., 2003; Martínez-Martínez and Azañón, 1997) (Fig. 5). They are described as asymmetric half  
220 grabens (Do Couto et al., 2014; Martínez-Martos et al., 2017; Pedrera et al., 2010, 2009) formed during the Upper  
221 Serravallian-Early Tortonian (Augier et al., 2005b; Augier et al., 2013; Meijninger and Vissers, 2006). Several of  
222 these NW-SE faults are active and cut across the metamorphic domes and the sedimentary basins (Augier et al., 2005a;  
223 Booth-Rea et al., 2004a; Giaconia et al., 2012; Montecat and Ott d'Estevou, 1999).

224 In addition to these structures, there are E-W right-lateral strike-slip fault zones and parallel depressions, like the  
225 Alpujarras fault zone between the Sierra de Gádor and the Sierra Nevada, and the Almanzora fault zone between the  
226 Sierra de los Filabres and Sierra de las Estancias (Fig. 5). The left-lateral Carboneras and Palomares fault system

Deleted: 2004

228 (Reicherter and Hübsher, 2006; Scotney et al., 2000) marks the tectonic limit with the Cabo de Gata volcanic province  
 229 (Fig. 5).  
 230 The domes are extension-related features interpreted either as 1) EW-metamorphic domes resulting from the  
 231 exhumation in the footwall of a regional W-directed extensional low-angle detachments, later folded during post-  
 232 Tortonian N-S contraction (Martínez-Martínez and Azañón, 1997; Martínez-Martínez et al., 2002, 2004) or 2)  
 233 Miocene metamorphic domes formed by constrictional ductile strain regime accompanying W-directed stretching of  
 234 the Alboran domain and trench retreat, with limited overprint by the Tortonian contraction ca. 8 Ma (Augier et al.,  
 235 2013; Augier et al., 2005; Augier et al., 2005b; Galindo-Zaldivar et al., 2015; Jolivet et al., 2021b; Martínez-Martínez  
 236 et al., 2002). Low-temperature constraints from the Nevado-Filabride and Alpujarride complexes confirm the west-  
 237 directed exhumation of the basement that occurred progressively from the Sierra de los Filabres at ~13-11 Ma  
 238 (Serravallian) in the East to the Sierra Nevada at 8-6 Ma (Late Tortonian-Messinian) in the West (Clark and Dempster,  
 239 2009; Janowski et al., 2017; Johnson et al., 1997; Platt et al., 2005; Reinhardt et al., 2007; Vázquez et al., 2011).  
 240

**Deleted:** e.g. Montenat & Ott d'Estevou, 1990; Sanz de Galdeano ...  
**Formatted:** English (US)  
**Deleted:** Vera, 1992; Sanz de Galdeano and Alfaro, 2004  
**Formatted:** English (US)  
**Deleted:** ; Martínez-Martos et al., 2017; Pedrera et al., 2010, 2007...  
**Formatted:** English (US)  
**Formatted:** Font colour: Black, English (US)



241  
 242 **Figure 5 :** Tectonic map of the eastern Betics showing the main structural elements in black after Augier et al. (2005)  
 243 and Do Couto (2014). CF: Carboneras Fault; PF : Palomares Fault.  
 244

245 Tectonic models for the formation of Neogene intramontane sedimentary basins vary depending on the prevailing  
 246 tectonic regime. EW-directed basins have been early described as pull-apart basins (e.g Alpujarran fault zone; Sanz  
 247 de Galdeano et al., 1985). Structural analyses then led to re-interpret these structures as transfer zones resulting from  
 248 differential extension between exhuming core-complexes (and detachment systems) since the Serravallian (13-11 Ma)

254 later refolded during Tortonian (9-8 Ma) compression in the Eastern Betics while extension is still active in the Central  
255 Betics (Martínez-Martínez et al., 2006). Other authors proposed that NE-SW extension lasted until 7.5-7 Ma in the  
256 Eastern Betics (Booth-Rea et al., 2004b; Giaconia et al., 2014).

Deleted: 2004

257 In support to the compressional stress regime in the Eastern Betics, Martínez-Martos et al. (2017) interpreted the E-  
258 W depressions are related to the tectonic reactivation of crustal weakness zone as dextral strike-slip faults in a  
259 counterclockwise rotation, accommodating part of the the N-S shortening. There are evidence that at the end of the  
260 Tortonian a regional uplift occurred, rising the remnants of late Tortonian marine platform, 7.2 Ma in age, to 1600 m  
261 above sea level in the Sierra de Gádor (Braga et al., 2003; Janowski et al., 2017), coincidentally with the onset of  
262 contraction in the Sierra Alhamilla and Sierra de los Filabres (e.g. Do Couto et al., 2014), in the Alboran domain (e.g.  
263 Martínez-García et al., 2017) and on the margins of the eastern Betic (Giaconia et al., 2013 ; 2015). In addition to  
264 shortening, this recent uplift may reflect deep mantle mechanisms like slab tearing or delamination (e.g. Duggen et  
265 al., 2003; García-Castellanos and Villaseñor, 2011; Mancilla et al., 2015a).

Deleted:

266 Based on the prevalence in some EW-trending basins, like the Huércal-Overa basin, of EW-trending normal faults,  
267 these basins have alternatively been interpreted as resulting from late exhumation stage of the domes, possibly as soon  
268 as the Serravallian, but mostly after the early Tortonian (syn-sedimentary faulting) (Augier et al., 2013; Augier et al.,  
269 2005b; Meijninger and Vissers, 2006). The NW-SE/NNW-SSE sedimentary basins (Guadix, Baza, Alhabia; Fig. 5),  
270 in contrast, are extensional basins formed parallel to the direction of the regional compression (Sanz de Galdeano and  
271 Vera, 1992; Larouzière et al., 1988). E-W strike-slip fault zones, aligned in the direction of the domes, and NW-SE  
272 normal faulting patterns are both key features consistent with predictions from models of oblique extension at  
273 transform margin (Fig. 3). Yet, based on existing structural and tectonic syntheses a clear temporal relationships  
274 between E-W ductile stretching in the domes and transcurrent deformation is not established (Fig. 5).

Formatted: Font colour: Black

Deleted: ¶

### 276 3.2 Is the Tortonian rift-related subsidence consistent with oblique extension ?

277 The stratigraphic architecture and depositional evolution of Tortonian intramontane basins provides first-order  
278 informations on the distribution of crustal thinning. Among the oldest sediments deposited unconformably on the  
279 Paleozoic-Triassic basement are the red alluvial conglomerates and deltaic series dated from the Serravallian to the  
280 Lower Tortonian (Fig. 6a). They are thicker and well exposed on the flanks of the Almanzora basin and on the northern  
281 Huércal-Overa basin (HOB), compared to the Alpujarras Corridor (AC) and Tabernas basin (TB) (Figs. 6 and 7a;  
282 Augier et al., 2013; Pedrera et al., 2010, 2007; Poisson et al., 1996). In the east of the Sorbas basin, it should be noted  
283 that Langhian-Serravalian deposits and perhaps sediments as old as Burdigalian have been locally reported (Giaconia  
284 et al., 2014).

Deleted: East

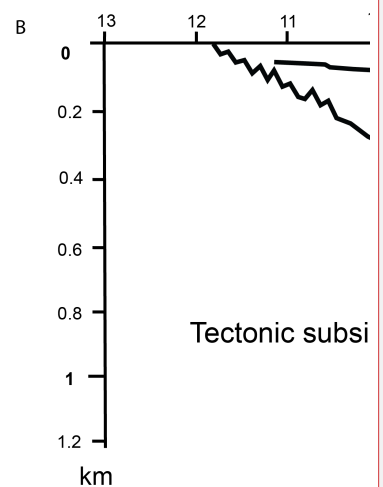
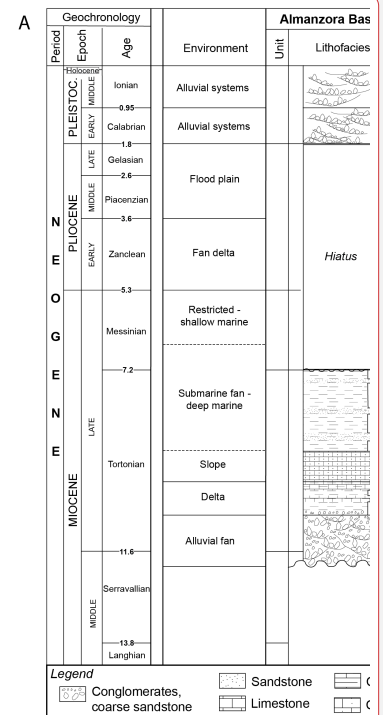
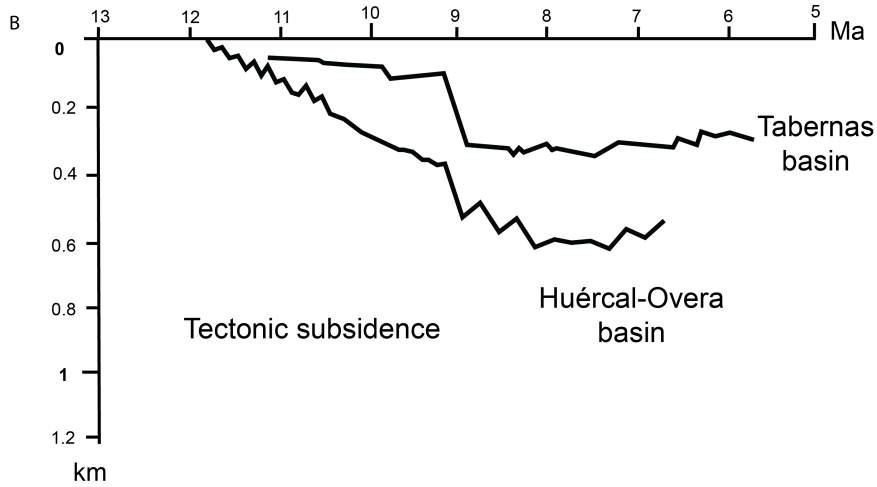
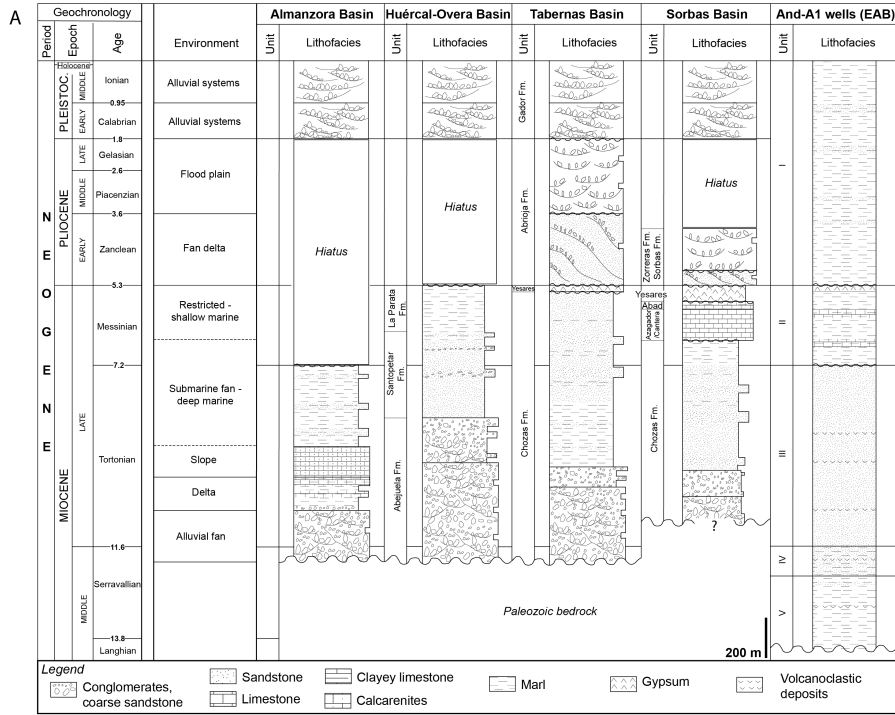
285 Paleogeographic reconstructions indicate that these Serravallian to Lower Tortonian sediments were deposited on a  
286 large emerged domain, stretching from Huercal-Overa to Granada, in the West and in Tabernas, to the South (Braga  
287 et al., 2003). Sourced from the Nevado-Filabride metamorphic complex (Hodgson and Haughton, 2004; Kleverlaan,  
288 1989; Meijninger and Vissers, 2006; Pedrera et al., 2010, 2007; Pickering et al., 2001; Weijermars et al., 1985) these  
289 deposits mark the onset of surface exhumation of the Sierra de Las Estancias and Sierra de Los Filabres.

294 During this initial stage, HOB is the most subsident basin (**Figs. 6b, 7a and 7b**), accumulating sediments at rates of  
295 400 m/Ma while rates are 140-180 m/Ma in the Tabernas basin (**Fig. 6b**) (Augier, 2005). Higher subsidence in the  
296 HOB, which also started earlier than in other basins, suggests extension occurred originally to the North associated  
297 with the exhumation of the Sierra de Las Estancias. Basal continental conglomerates are overlain by grey coarse-  
298 grained Tortonian sandstones found occasionally, e.g. in the Almanzora basin, intercalated with marine marls (**Figure**  
299 **6a**). They are topped by mid-Tortonian bioclastic calcarenite and coral reefs (Braga et al., 2003; Martin et al., 1989;  
300 Pedrera et al., 2007).

301 During the same interval, TB recorded the deposition of 300 to 400 m of coarse to medium-grained deltaic marine  
302 clastics overlying unconformably the lowermost red series (**Fig. 6a**). These sediments pass upwards, e.g. in TB, to  
303 deeper marine 1200 m-thick turbiditic and marls series intercalated with regional-scale megabeds, revealing the onset  
304 of rapid tectonic subsidence (Haughton, 1994; Kleverlaan, 1989, 1987; Pickering et al., 2001; Weijermars et al., 1985).  
305 Details of depositional architecture of the Tortonian suggest that part of this subsidence evolution was controlled by  
306 E-W dextral strike-slip faults (Haughton, 2000 ; Baudouy et al., 2021) under transtensional strain.

307 The transition from continental to deep marine sedimentary environments (water depth of 400-600 m according to  
308 Poisson et al., 1999) witnesses the rapid rift-related tectonic subsidence achieved during the upper Tortonian times  
309 (~9 Ma; **Figs. 6 and 7c**) (Augier et al., 2005b; Montenat and Ott d'Estevou, 1992; Weijermars et al., 1985). At around  
310 8 Ma, accumulation rates drop by a factor of two to 200 m/Ma in HOB and 70 m/Ma in TB, revealing a marked  
311 reduction in subsidence. Subsidence then became negative as basement uplifted from around 7 Ma (**Figs. 6b and 7d**)  
312 in both TB and HOB.

313  
314

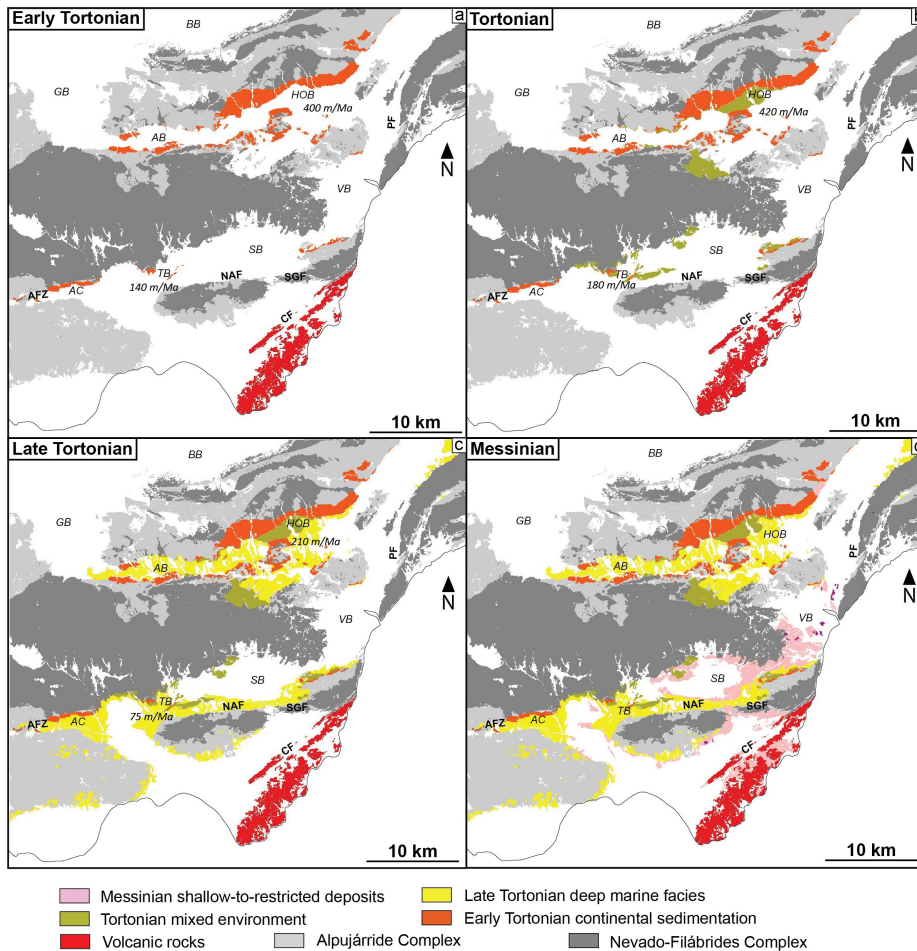


Deleted:



317 **Figure 6** : Stratigraphic evolution and lithologies of intramontane basins in the eastern Betics and offshore A1 well.  
318 (a) Neogene stratigraphy and basin-fill correlation in the Almanzora and Huércal-Overa basins (Mora, 1993), Tabernas  
319 basin (Hodgson and Haughton, 2004; Kleverlaan, 1989; Pickering et al., 2001) and Sorbas basin (Fortuin and  
320 Krijgsman, 2003; Martin and Braga, 1994; Riding et al., 1998). Middle Miocene sedimentary environments in the  
321 Alboran Sea are after (Comas et al., 1992). (b) Neogene tectonic subsidence evolution for Tabernas basin and Huércal-  
322 Overa basin are from Augier (2004). The curves are obtained from backstripping techniques incorporating eustatic  
323 and paleobathymetric corrections. Question mark beneath the Sorbas basin lithofacies column indicates the potential  
324 for uncertainty/variability across the basin (see text).  
325

326 The geometry of the Almanzora (Pedrera et al., 2009), Sorbas (e.g. Do Couto et al., 2014) and Huércal-Overa basin  
327 basins (Pedrera et al., 2010) inferred from gravity measurements indicate that these basins are asymmetrical and  
328 deepening southwards. This sediment infill pattern recalls the formation of asymmetrical basins predicted by  
329 numerical models of flexural strike-slip basins (Neuharth et al., 2021). According to this model, the asymmetry  
330 observed should reflect the development of strike-slip basins loaded by sediments originated from the North. In  
331 addition, a larger subsidence in HOB is an indication of abrupt crustal thinning to the south of Sierra de las Estancias  
332 where the crustal thickness is the largest (**Fig. 2**). Therefore, at least the Serravallian-Tortonian infill patterns agree  
333 with oblique extension.  
334



335  
 336 **Figure 7:** Distribution of (a) lower Tortonian, (b) Tortonian, (c) upper Tortonian and (d) Messinian deposits based on  
 337 geological mapping of the different basins. CF: Carboneras Fault; PF : Palomares Fault; SGF: South Gafarillo fault;  
 338 NAF: North Alhamilla fault; AFZ: Alpujarras fault zone; BB: Baza basin; GB: Guadix basin; AB: Almanzora basin;  
 339 HOB: Huercal-Overa basin; VB: Vera basin; SB: Sorbas basin; TB: Tabernas basin; AC: Alpujarras Corridor.  
 340

Deleted: P

341 **4. Brittle faulting : pure extension versus transtensional deformation in Neogene basins**

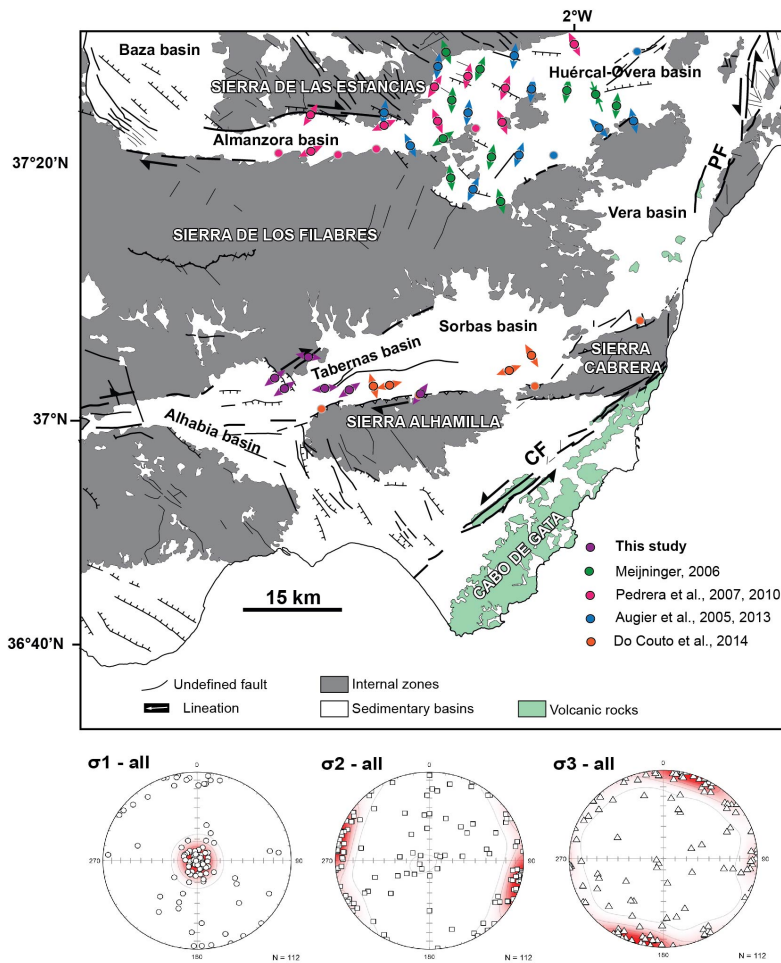
342 **4.1. Tectonic regime in the eastern Betics**

343 **Figure 8** presents a compilation of 112 fault slip data inversion previously analysed in the eastern Betics combined  
 344 with new measurements conducted in the Alpujarras Corridor and in the Tabernas basin (**Table S1**). Most faults are  
 345 syn-Tortonian or cut through the Tortonian. This compilation emphasizes a regional trend of  $\sigma_3$  stress axes oriented

347 NNE-SSW (N20°E) with subordinate  $\sigma_3$  oriented E-W. In details, this well-defined regional horizontal extension  
348 reflects a combination of pure normal faulting regime ( $\sigma_2$  horizontal and oriented NW-SE/WNW-ESE, 73% of stress  
349 tensors) and strike-slip faulting regime ( $\sigma_2$  vertical to steeply-dipping and  $\sigma_1$  horizontal an striking NNW-SSE, 27%  
350 of stress tensors). N-S to NW-SE compression is also reported in the HOB associated with incipient synform and  
351 depocenter which is dated to the lower Tortonian coeval with the prominent EW/WSW-ENE extension (e.g. Pedrera  
352 et al., 2010).

353 We describe below, based on a selection of outcrops in the vicinity of the contact between Tortonian basins and major  
354 metamorphic domes, the expression of EW and NW-SE extensional faulting in the field. We then discuss how they  
355 are linked to the regional stress regimes.

356



357  
358  
359  
360  
361  
362  
363  
364

**Figure 8:** Synthesis of stress regimes resolved from fault slip data inversion in Tortonian basins. Color-coded circles with arrows depict tectonic sites where extension (given as arrows) is horizontal (pure extensional or strike-slip stress regimes). Sites where reverse tectonic regimes prevail are shown as circles highlighted in grey. Below, stereoplots of paleostresses  $\sigma_1$ ,  $\sigma_2$  and  $\sigma_3$  show a compilation of all brittle tectonic regimes extracted from Table S1. Collectively they define a prominent extension oriented NNE-SSW with a subordinate E-W-striking extension. CF: Carboneras Fault; PF: Palomares Fault.

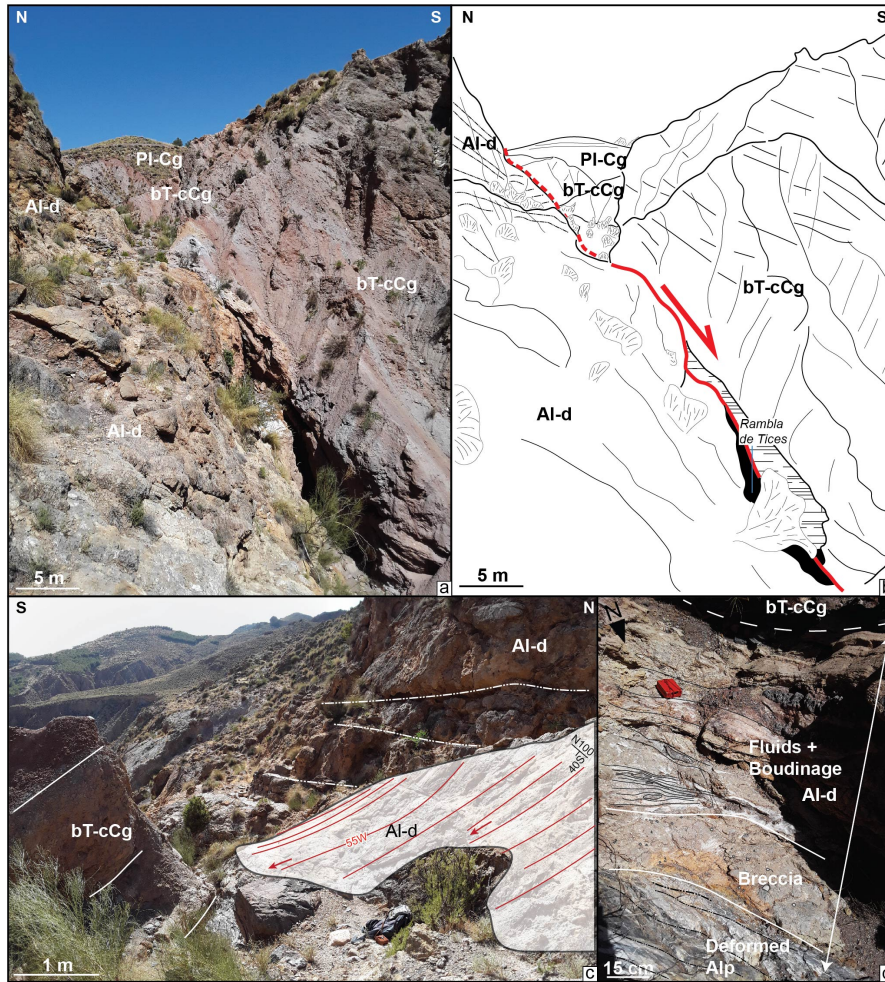
365 **4.1 EW-trending faults: evidence for pre-Tortonian oblique extension ?**

366 In Tortonian intramontane basins, one of the main set of faults is represented by E-W-directed faults, including ENE-  
367 WSW to ESE-WNW sets. North of the Alpujarras Corridor (AC), 3 km to the NE of Canjáyar, the contact between  
368 the basal Tortonian conglomerates and the series of Alpujarride complex is exposed in the Rambla de Tices. It is

Deleted: directed faulting

370 shaped by a 2-meter thick fault zone (Figs. 9a,b) striking N100°E, which has a normal sense of slip with a right-lateral  
371 strike-slip component (Fig. 9c). It consists of cataclastic breccias and sheared blocks (boudins) of the host rocks (Fig.  
372 9d). This major fault is found along the 65 km-long Alpujarras fault zone described by Martínez-Martínez (2006) as  
373 a major strike-slip dextral transfer zone south of the Sierra Nevada that accommodates both WSW-extension and dextral  
374 movement. It is mechanically consistent with NE-SW/ENE-WSW extension under a strike-slip regime as resolved  
375 nearby along the same faults system (Martínez-Martínez, 2006). Fig. 9 indicates the fault is parallel to the basal  
376 Tortonian series but cuts across the Alpujarride complex. In the HOB, on the southern flank of the Sierra Limaria  
377 (Fig. 8), the unconformity between the lower Tortonian red conglomerates and the Alpujarride units (Rambla de  
378 Cordoba, 2km NW Arboleas, Figs. S1a, b) is found reactivated as a normal fault with a dextral shear component.  
379 To the North of TB, a large morphological surface presents a rare exposure of the micaschist basement of the Nevado-  
380 Filabrides complex allowing the study of deformation on the southern flank of the Sierra de los Filabres (Fig. 10). The  
381 deformed NF series shapes a kilometric-size antiform with axial planar surface dipping towards the North. The steeply-  
382 dipping cleavages directed NE-SW on its southern flank are deformed by numerous dextral shear zones with lengths  
383 ranging from 100 m to less than 5 m (Fig. 10b, c). In addition to isoclinal folds parallel to the main foliation that are  
384 clearly associated to an early stage of ductile EW-stretching, we recognize close to the strike-slip shear zones, steeply-  
385 dipping metric-size open to tight folds inclined to the NE (Fig. 10d). To the south, Tortonian conglomerates are  
386 overlying unconformably the folded NF foliation. This stratigraphic relationships and the average low dip of Tortonian  
387 strata (20°SE) indicate that strike-slip deformation occurred before the deposition of Tortonian conglomerates and  
388 after the tilting of the NF foliation (see cross section in Fig. 10a). This argues that the transition from HP  
389 metamorphism (Burdigalian-Langhian) in the NF (Platt et al., 2006) to W-directed ductile crustal thinning and right-  
390 lateral strike-slip faulting occurred before the Tortonian, most likley around the Serravallian at 12-13 Ma. This interval  
391 is considered to mark the transition from ductile to brittle extension in the region (e.g. Augier et al., 2013). Because  
392 strike-slip faulting postdates folding of the NF foliation, and are consistent with WSW-ENE oblique extension, we  
393 suggest that the Sierra de los Filabres metamorphic dome formed in a transtensional strain regime. This hypothesis  
394 conforms with prediction of transtension at the tip of the STEP fault (Le Pourhiet et al., 2012) and with model of  
395 oblique extension (see Fig. 3).  
396

- Deleted: extension in the metamorphic domes known to have started in the Burdigalian
- Deleted: the
- Deleted: Langhian-
- Deleted: (
- Deleted: -14
- Deleted: ).
- Deleted: often



405  
 406 **Figure 9.** (a) and (b) Fault zone at the contact between the Tortonian basal conglomerates and the series of the  
 407 Alpujarride complex south of AC (Rambla de Tices, see Fig. 5 for location). (c) slickensides on the fault zone reveal  
 408 a normal sense of slip with right-lateral strike-slip component found in association with (d) cataclastic breccias,  
 409 sheared boudins of metamorphic and sedimentary rocks. Al-d: Alpujarride dolomites; bT-cCg: basal Tortonian  
 410 continental Conglomerates; PI-Cg: Pliocene Conglomerates. Coordinates 37.031944°N/-2.716274°E.

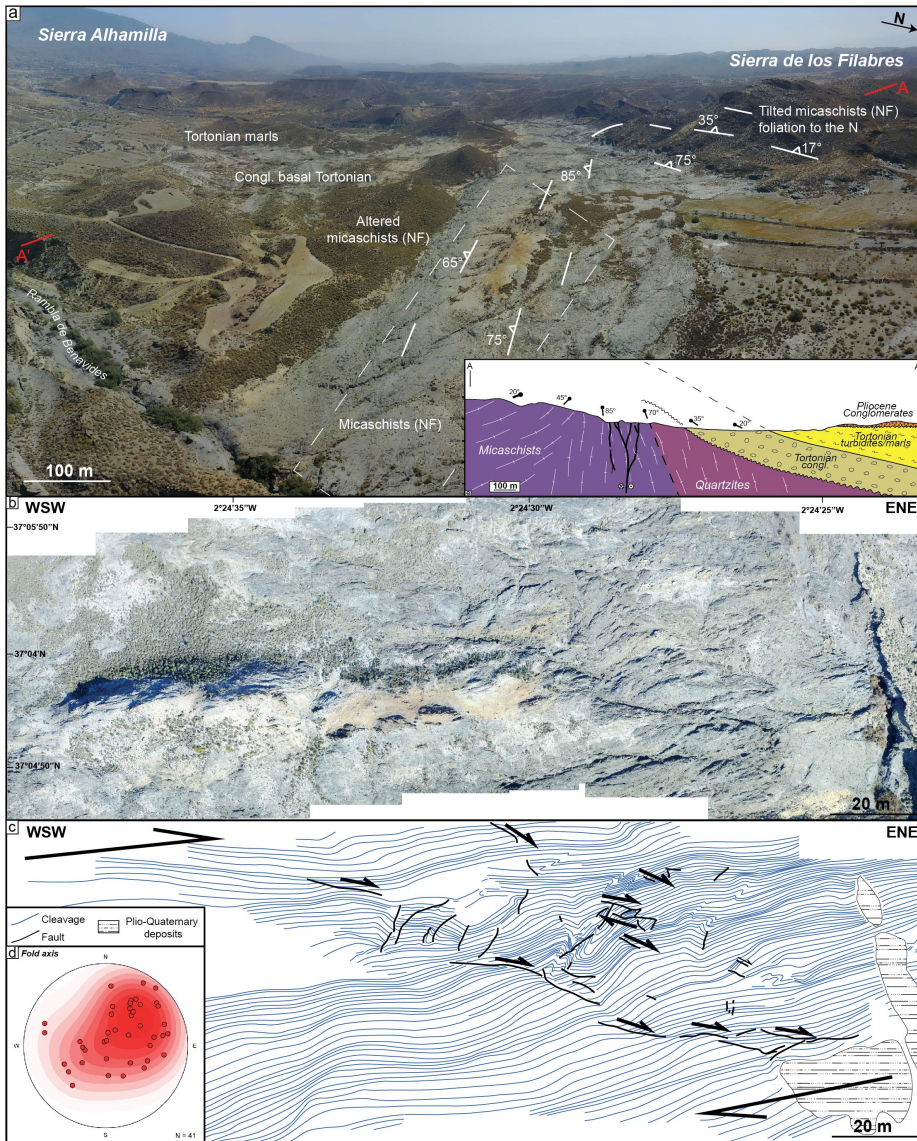
412 **4.1.2. NW-SE-trending normal faults**

413 A second set is represented by NW-SE directed normal faults (Fig. 8). They are found, for instance, bordering the  
 414 NE part of Alhabia basin, where they cut across the basement and interrupt the westward continuity of the southern

Deleted: directed  
 Deleted: faulting

417 flank of the Sierra de los Filabres. One major fault zone of this system is well exposed in the Arroyo del Verdelecho,  
418 7 km to the west of Tabernas, on the eastern border of the Alhabia basin (**Figs. 11 and S2**). From a regional point of  
419 view this large NW-SE fault zone controls the deepening of the Tortonian basin and the position of Pliocene  
420 depocenter in its hangingwall, towards the West. NW-SE normal faults also cut across the lower Tortonian  
421 conglomerates in the hangingwall but their throw diminishes upward in the upper Tortonian margin sediments,  
422 suggesting fault activity during the late Tortonian (**Fig. 11**). One major fault zone is outlined by cataclastic breccias  
423 made of marbles originated from the exhumed Alpujarride complex in the Sierra de los Filabres (**Fig. S2**).  
424 South of HOB (south of Arboleas), NW-SE faults are seen cutting through the late Tortonian sands and marls series,  
425 indicating that NE-SW extension is at least Tortonian (**Figs. S1c, d**).  
426





427

428

429

430

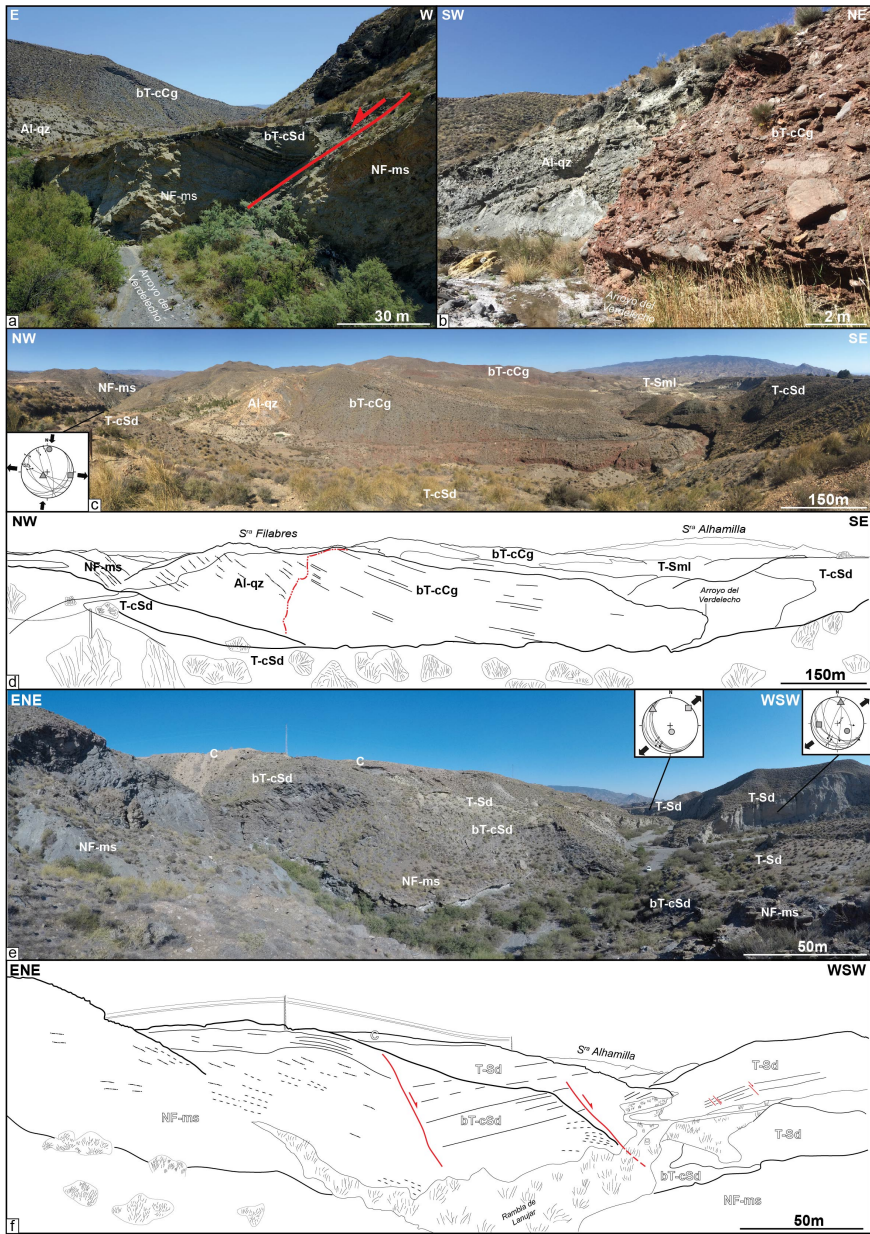
431

432

**Figure 10** : (a) Drone view taken in the SSW direction of the southern flank of the Sierra de los Filabres at the contact with the Tabernas basin (see Figure 5 for location). Local folding of the micaschist is apparent in the right where the foliation is striking NNE-SSW and is dipping  $\sim 25^\circ$ E whereas it is vertical and striking SW-NE in the center of the studied area forming paleosurface. Local cross section highlights the unconformable contact between the Tortonian conglomerates and overlying on the basement. (b) High-resolution drone images of the paleosurface and (c) line-

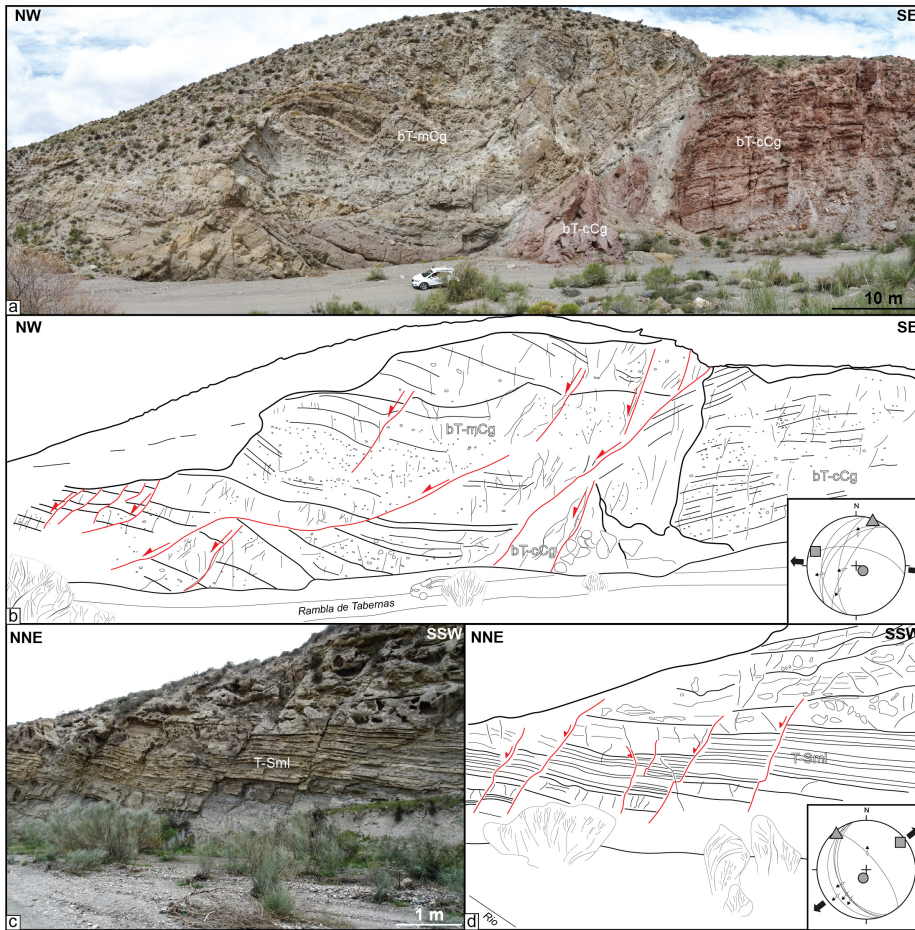


433 drawing of the foliation revealing secondary folding (see **(d)** stereoplot of fold axes inclined to the NE) and dextral  
434 shear zones. Coordinates 37.082777°N/-2.410544°E.  
435  
436  
437



439 **Figure 11** : (a) Field photographs of a NW-SE normal fault at the contact between the Nevado-Filabride micaschists  
440 (footwall) and Tortonian sediments (hangingwall). (b) Stratigraphic contact between grey and red basal Tortonian  
441 continental conglomerates. These thick Tortonian series rest conformably on the Alpujarride complex (c, d).  
442 Coordinates 37.059507°N/-2.478386°E. (e, f) NW-SE normal faults cutting across the NF micaschists basement.  
443 These faults that also affect the early Tortonian deposits are sealed by late Tortonian deposits and are therefore syn-  
444 depositional. See Figure 5 for location. Al-qz: Alpujarride quartzites; NF-ms: Nevado-Filabride micaschists; bT-cCg:  
445 basal Tortonian continental Conglomerates; bT-cSd: basal Tortonian continental Sandstones; T-cSd: Tortonian coarse  
446 Sandstones; T-Sd: Tortonian Sandstones; T-Sml: Tortonian Sandstones-marls; C: calcretes. Coordinates  
447 37.061279°N/-2.490309°E. Paleostress orientations are in Table S1.  
448

449 Both fault slip data and our own observations argue for a regional pre-Tortonian and syn-early Tortonian NNE-SSW  
450 directed extension. This direction of extension is also found associated with less well-developed strike-slip regimes  
451 (Fig. 8). It is consistent with the D1-D2 phase of brittle deformation found in HOB (Augier et al., 2013). The fact that  
452 extension and strike-slip regimes occurred synchronously, or overlap rapidly in time, supports the view that they  
453 reflect the same large-scale tectonic setting. The reason why strike-slip faulting is less apparent in the field than  
454 expected in models in Fig. 3 is likely to reflect the fact that oblique extension is not fully partitioned between normal  
455 and strike-slip components and is actually distributed along oblique structures. Moreover, where strike-slip faults are  
456 found they are associated with narrow basins or near the contact between the cover and basement but not in the center  
457 of HOB or TB. The NNE-SSW to NW-SE faults appear to postdate the deposition of the early Tortonian red  
458 conglomerates and is synchronous with the deposition of marine Tortonian series (Fig. 12). These normal faults  
459 currently form half-graben filled with Plio-Quaternary deposits (Guadix, Baza, Alhabia) and are active today. But the  
460 importance of extension-related brittle deformation over brittle compression decreases eastwards. Indeed, a late brittle  
461 compressional event oriented roughly N-S is described in the literature as a D3 brittle event (e.g. in HOB) associated  
462 with reverse and strike-slip faults (Augier et al., 2013). The post-late Tortonian shortening is seen responsible for fold  
463 amplification and reverse faulting on the northern limb of Sierra de Alhamilla and Sierra de los Filabres, and locally  
464 in the eastern part of the HOB near the termination of left-lateral strike-slip faulting evolution of the Alhama de Murcia  
465 fault (Fig. 8).



466  
 467 **Figure 12:** (a, b) N-S to NNE-SSW-oriented normal to dextral faults affecting the basal Tortonian continental  
 468 conglomerates (bT-cCg) and marine conglomerates (bT-mCg) (Rambla de Tabernas). They form a long and tight E-  
 469 W anticlinal crosses the Tabernas basin (see Figure 5 for location). (c, d) Several normal faults observed in Tortonian  
 470 sandstones and marls (T-Sml). They are mostly oriented NNW-SSE. Coordinates 37.041648°N/-2.399318°E.  
 471 Paleostress orientations are in Table S1.

472 **5. N-S crustal-scale section across the oblique/transform margin of Alboran basin**

473 To examine further the structural relationships between extension and strike-slip faulting across the Alboran margin,  
 474 we explore 2D multichannel seismic lines acquired during the MARSIBAL 1-06 cruise (Comas and MARSIBAL1-  
 475 06 Scientific Party, 2007) and ESCI cruises (Comas et al., 1995) across the Eastern Alboran basin (EAB). The studied  
 476 seismic dataset consists of ~300 km and are deep-penetration multichannel seismic reflection studies (12 s two-way  
 477 travel time - TWTT). Here, we study two lines namely MSB08 and MSB07 (see location in Fig. 1). For stratigraphic

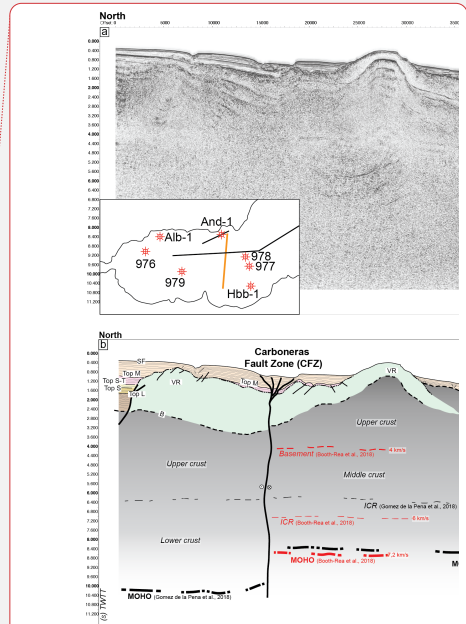
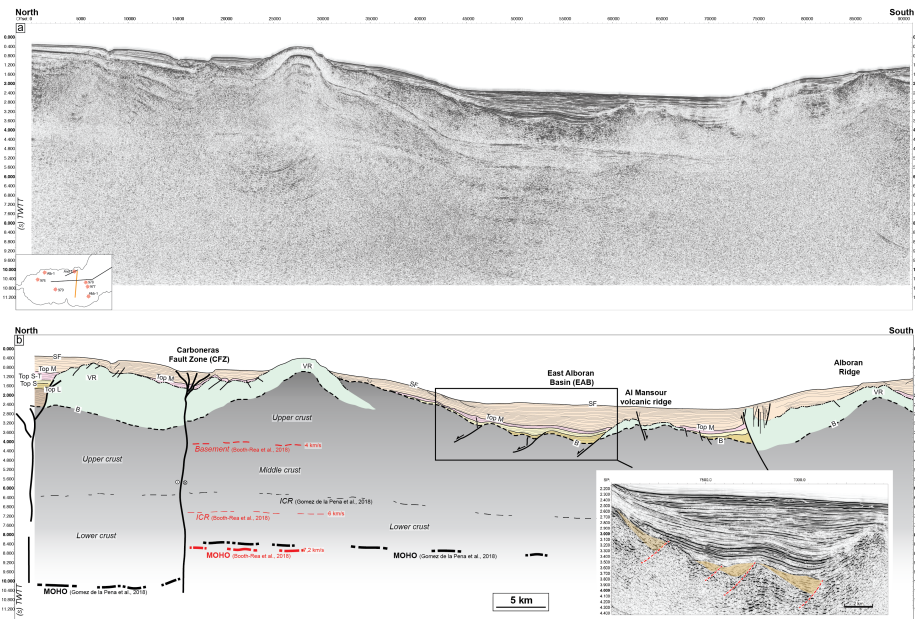


478 and structural correlations between the studied seismic lines, we used the Andaluca-A1 well (Fig. 6a) and results  
 479 from ODP 977 and 978 legs (see location in Fig. 1). MSB08 is striking N70°E, slightly oblique to the shoreline. It is  
 480 close, and runs parallel, to TM08 line of Gómez de la Peña et al. (2018). It is calibrated by Andaluca-A1 well and  
 481 ESCI-Alb1 line (Comas et al., 1995). Line MSB07 stretches in the N-S direction between the EAB in Spain and SAB  
 482 to the north of Morocco parallel to line TM09 (Gómez de la Peña et al., 2018) and crosscuts line ESCI Alb2b  
 483 presented in Comas et al. (1995) and Booth-Rea et al. (2007) (Fig. 1).  
 484

485 **5.1 Offshore structures and stratigraphic architecture**

486 The Carboneras Fault is well imaged north of MSB07 (Fig. 13). It forms a negative crustal-scale flower structure  
 487 related to left-lateral strike-slip faulting that involves a Moho depth variation between 12 s to 9-8 s TWT after Gómez  
 488 de la Peña et al. (2018). It separates a thin continental crust to the North (25-20 km; Fig. 2), from the magmatic calc-  
 489 alkaline arc crust of the EAB with a thickness of 18 km in the south (Booth-Rea et al., 2007, 2018; Gómez de la Peña  
 490 et al., 2018, 2020a).  
 491

- Deleted: positive
- Deleted: antiformal
- Formatted: English (US)



Deleted:

492  
 493 **Figure 13** : Seismic reflection line MSB07 (location on Fig. 1). Discontinuous intracrustal reflectors (ICR) imaged  
 494 between 3 and 6.5 s TWT, have been interpreted as mylonitic zones within the metamorphic basement (Carbonell et  
 495 al., 1998; García-Dueñas et al., 1994; Gómez de la Peña et al., 2018). VR: Volcanic Ridge; B: Acoustic basement;  
 496 Top L : Top Langian; Top S: Top Serravallian; Top S-T: top Serravallian-Tortonian; Top M: Top Messinian; SF:  
 497 Seafloor.

501  
502  
503  
504  
505  
506  
507  
508  
509  
510  
511  
512  
513  
514  
515  
516  
517  
518  
519  
520  
521  
522  
523  
524  
525  
526  
527  
528  
529  
530  
531  
532  
533  
534  
535  
536  
537  
538

Reflection seismic data (Figs. 13, 14, 15) collectively show a stratified crust, corresponding to the sediment cover, down to 2.4-4 s TWT, which outlines the acoustic basement with high reflectivity (B). Locally, the top basement reflector coincides with erosional palaeo-relief or high angle normal faults bounding basement highs. These faults are oriented mostly NW-SE to NE-SW and cut across the basement. We recognized on seismic images magmatic additions in the continental crust that are shaped by volcanic edifices exposed on the seafloor (e.g. Chella Bank) or slightly buried (Alboran Ridge) outlined by symmetric downlaps and onlaps of sediments. These constructions form topographic highs such as the Chella Bank on the MSB08 line (Fig. 14), the Alboran Ridge on the MSB07 line (Fig. 13) and the Maimonides Ridge on the ESCI-Alb2b line (Fig. 15). All the reflectors corresponding to layers as old as Tortonian are onlapping against the volcanic ridges confirming that the volcanic activity occurred during the middle to late Miocene times, which is shown by Duggen et al. (2008). Some reflectors up to the top Messinian (top M) onlap onto the volcanic ridges probably as a result of Pliocene uplift.

The stratigraphy offshore, on the continental crustal domain, is defined by the recognition of five seismic stratigraphic units in Andaluçia-A1 well (Jurado and Comas, 1992) labeled I-V from top to base (Figs 6 and 16) and separated by unconformities. The seismostratigraphic units I to V vary in thickness (Fig. 16) and their architecture is conditioned by the occurrence of basement highs and crustal-scale faults.

Below the Miocene sedimentary filling, Andaluçia-A1 well reveals ~190m of phyllitic and quartzitic meta-sediments (2.4 to 4 s TWT below the Alboran basin, Figs. 13 and 14) topped by Langhian to Tortonian marls (top at ~1.6 to 3.4 s TWT below the Alboran basin) interbedded with Tortonian-Messinian tuffs and basaltic lavas. These units have been correlated in the magmatic arc crust of EAB after Gómez de la Peña et al. (2020b). The older deposits (Unit V) Langhian-Serravallian in age, consist of clays and marls with intercalated sands and volcano-clastic deposits. The seismic facies of this Unit V is made of moderate amplitude and low frequency discontinuous reflections packages (Figure 16), and is only present in the Northern Alboran Basin. They are correlated with volcanic series in the EAB (vY3) (Gómez de la Peña et al., 2020b). They pass upward into Serravallian sand-silty clay turbidite (Unit IV) possibly correlated with volcanic series in EAB (vY2 after Gómez de la Peña et al., 2020b). This unit exhibiting low to moderate amplitude, moderate frequency drawing continuous sheeted to disrupted reflectors, is unconformably overlying Unit V and locally onlaps onto the basement. Thickness of Unit IV remains rather thin in the North and East Alboran Basin. It can't be properly identified in the South Balearic Basin, east of the Maimonides volcanic ridge (Fig. 15). The Unit III dated from late Serravallian to late Tortonian is represented by sandstones interbedded with volcano-clastic levels which correlates in EAB with volcanics vY1 unit. Unit III contains internal reflections characterized by low to moderate amplitude, moderate frequency continuous sheeted reflectors. Its thickness remains relatively constant from the NAB to the EAB, and is identified beneath the Messinian Unit II in the South Balearic Basin. Unit II corresponds to the Messinian evaporite, carbonate, volcanic, and volcanoclastic deposits interbedded with fine-grained sediments and is equivalent to unit III of Gómez de la Peña et al. (2020b) in EAB. Seismic facies of Unit II is marked in the Alboran domain by lower amplitudes and lower frequency reflectors. In ESCI-Alb2b line, Unit II increases drastically east of the Maimonides ridge, which delimits the western boundary of the salt deposits in the Western Mediterranean basin

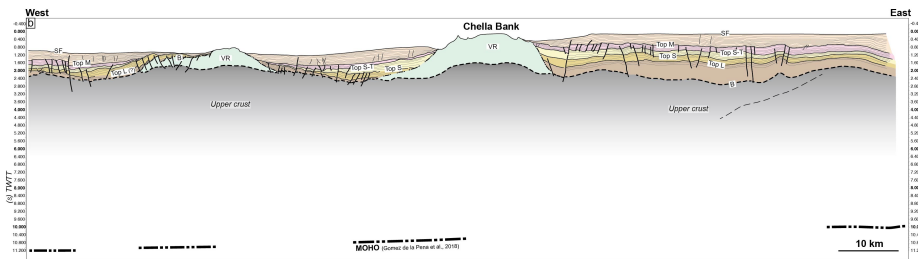
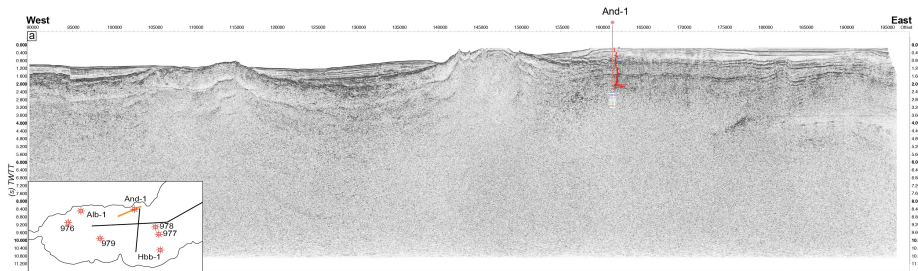
Deleted: 18

540 during the Messinian Salinity Crisis (Haq et al., 2020). Unit II is topped by Unit I made of Pliocene to Quaternary  
 541 clays and sanstones, which are correlated with units II and I in EAB (Gómez de la Peña et al., 2020b). Unit I is marked  
 542 by thinly bedded, mostly parallel, high-frequency and low amplitudes reflectors (Fig. 15). Its thickness fluctuates in  
 543 response to sedimentary processes (Juan et al., 2016).

544 Along line MSB08 (Fig. 14) the Langhian-Serravallian (Unit V) is maximum 1600 m-thick (using a P-wave velocity  
 545 of 3.2 km/s calculated within Andaluca-A1 well). In EAB, south of Carboneras Fault Zone, the total thickness of Unit  
 546 V is only ~300 m on MSB07 (Fig. 13) and is absent in ESCI-Alb2b (Fig. 15). The Serravallian-Tortonian (Unit IV-  
 547 III) interval shows only very limited sediment accumulation (~300 m) except near the NW-SE oriented normal faults  
 548 where growth geometries are visible. These normal faults are sealed by the Tortonian-Messinian deposits, indicating  
 549 a syn-sedimentary faulting during the middle Miocene (Fig. 13). With respect to onshore observations this  
 550 sedimentary infill is more continuous and is also much thinner compared to TB and HOB where they are represented  
 551 by thick conglomerates and marls/turbidites (> 1km) (Fig. 7), and they are eroded or not deposited along the axes of  
 552 the metamorphic domes. The Messinian deposits (Unit II) are ~150-350 m-thick north of CF (MSB07-08 ; Figs. 13,  
 553 14) and increase to about 1200 m eastward in the eastern EAB (ESCI-Alb2b ; Fig. 15), and in Algero-Balearic basin  
 554 (Gómez de la Peña et al., 2020b). The top Messinian reflector is topped by thick horizontal sedimentary strata, with a  
 555 maximum thickness of 1.2 s TWT (~2.4 km assuming a velocity of 2 km/s) on line MSB07, suggesting an important  
 556 channel system during the Pliocene.

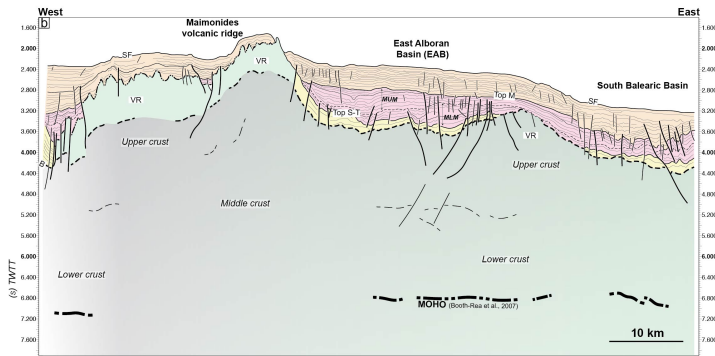
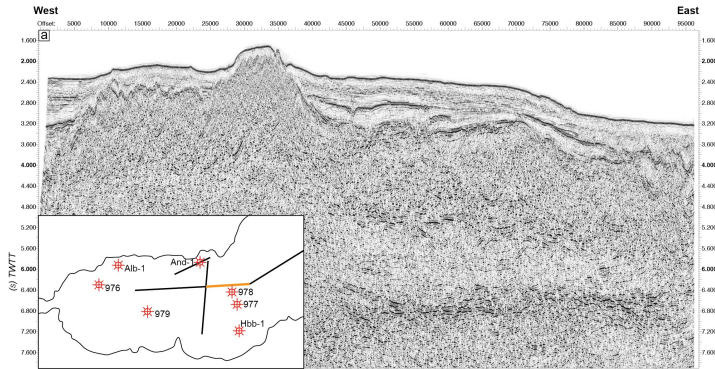
557 The Pliocene-to-Quaternary series are poorly deformed except in the vicinity of CF and near the Alboran Ridge where  
 558 this is associated with south-dipping reverse fault (Fig. 13). This late and still active compressional tectonics is  
 559 revealed by the overthrusting of the SAB over the south margin of the EAB (e.g. Martínez-García et al., 2011).

560



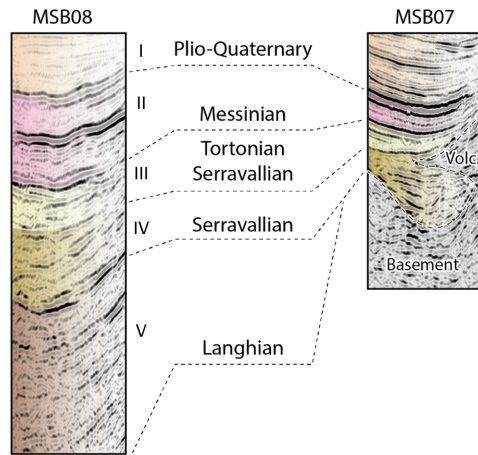
561

562 **Figure 14** : Seismic reflection line MSB08 (see location on **Fig. 1**). See Figure 13 for abbreviations. See also Figure  
 563 S3 showing a zoom on the main seismic facies recognized in Andalucia-A1 well.  
 564



565 **Figure 15. (a, b)** Seismic reflection line ESCI-Alb2b and interpretation (see Figure 1 for location). Seismic units are  
 566 correlated with those defined by Booth-Rea et al. (2007). See Figure 13 for abbreviations.  
 567  
 568  
 569





570  
 571 **Figure 16** : Seismic facies of units I to V seen through seismic lines MSB08 close to the shoreline and the line  
 572 MSB07, located deeper in the East Alboran Basin.

573 **5.2 N-S crustal cross-section of the Alboran margin accounting for strike-slip faulting**

574 Based on subsurface constraints and field data, we present in Figure 17 a crustal-scale section across the rifted margin,  
 575 from the Sierra de las Estancias and Huercal-Overa basin (HOB) to the Alboran ridge that represents the inverted  
 576 southern margin of the EAB (Fig. 17). The proximal margin, where the crust is 30-35 km-thick, is defined to the North  
 577 by the transition between the south Iberia margin, and the metamorphic domain of the Alboran basement exposed in  
 578 the Sierra de las Estancias. This continental domain preserves part of the crustal thickness acquired during former  
 579 Betic orogenic phase that has been little involved in crustal thinning. The onset of crustal thinning to the south  
 580 coincides with the position of the lithospheric tear fault documented by seismology (Fig. 4; Mancilla et al., 2015a)  
 581 and is recorded by the formation of asymmetric basins of the HOB and TB, shaping the upper neck domain. Orthogonal  
 582 and oblique extension in this domain is accommodated by normal and strike-slip faulting during the Tortonian. From  
 583 the Sierra de los Filabres to the south, the thickness of the continental crust reduces to 25 km in the Tabernas basin  
 584 along the Alpujarras strike-slip fault zone and below the Sierra Alhamilla (Fig. 17). The Nijar basin depicts the  
 585 transition towards offshore distal domains where the continental crust reaches a thickness of 20 km. The Tortonian  
 586 and Messinian marine sediments are also thicker. It is worth noting that a number of volcanic bodies offshore (e.g.  
 587 Chella Bank on MSB08) accompany crustal thinning of the continental crust. The Carboneras Fault (CF) brings crusts  
 588 with different thicknesses and composition into contact. South of CF, the crustal thickness of the EAB is 18 km and  
 589 seismic velocities, especially the occurrence of a high-Vp lower crust, has been considered to indicate the EAB is  
 590 floored by a magmatic arc crust (Gómez de la Peña et al., 2018; 2020), formed in a supra-subduction context above  
 591 the subducting Alboran slab (Booth-Rea et al., 2018). The crustal thickness of the EAB is compatible with crustal  
 592 thinning of the continental margin, and the occurrence of NW-SE-trending faults also recognized onshore despite  
 593 being slightly older (Serravalian-Tortonian) suggest that the EAB formed under the same back-arc extension setting.

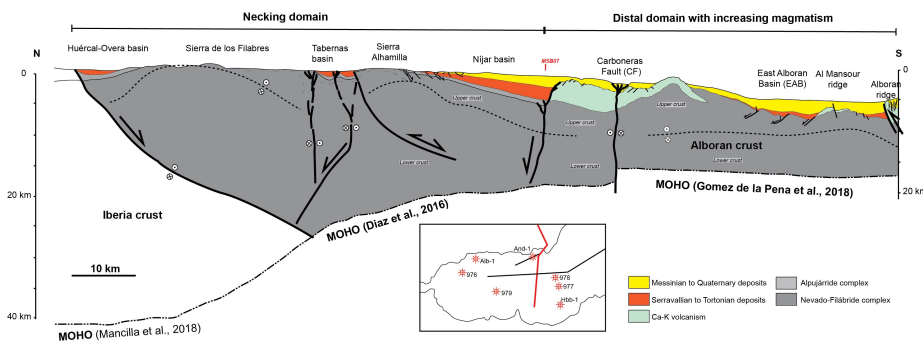
594 relative to westward slab retreat as the whole Alboran margin did. Thus, the magmatic arc crust of the EAB could  
 595 represent voluminous magmatic intrusions (e.g. Al Mansour dacite, Alboran Ridge rhyolite dated to ca. 9 Ma; Duggen  
 596 et al., 2004; [Tendero-Salmerón et al., 2022](#); **Fig 17**) formed on the distal rifted margin of Alboran. The investigation  
 597 of the causes of calc-alkaline magmatism is beyond the scope of this study, but we suspect it reflects post-subduction  
 598 arc magmatism induced by remelting, during extension **and** delamination, of a metasomatized wedge of mantle  
 599 lithosphere formed during a previous subduction event (e.g. Richards, 2009). Crustal shortening in **Figure 17** is  
 600 distributed across north-vergent reverse faults below the Alboran Ridge, on the northern limb of Sierra de Alhamilla  
 601 **and CF strike-slip fault zone.**

~~Deleted: or~~

~~Deleted: be~~

~~Deleted: the CF and EBSZ strike-slip fault zones,~~

~~Deleted: and~~



602  
 603 **Figure 17.** Crustal-scale cross section of the Alboran margin in the eastern Betics interpreted based on onshore and  
 604 offshore constraints presented in the text. Note that in the necking domain the extension of faults downwards to  
 605 Moho depths is not imaged on the seismics and therefore largely inspired by inferences from 3D numerical models  
 606 (see Fig. 3).  
 607  
 608

613 **6. Implications**

614 The question of whether the Miocene tectonic evolution of the Betics reflects crustal thinning associated with oblique  
615 back-arc rifting as suggested from present-day strain patterns is unclear in the literature. We found based on a  
616 comparison between numerical models and basin analyses, fault kinematics and structure of the margin in the eastern  
617 Betics compelling evidences that crustal thinning was controlled by oblique extension. Oblique rifting operated since  
618 at least the middle Miocene in relation with Alboran slab retreat below the Alboran basin and is kinematically  
619 associated with slab tearing and delamination below the central and eastern Betics.

620 One of the most striking tectonic feature of the Alboran margin (Fig. 17) is the abrupt N-S crustal thinning oblique to  
621 the direction of slab rollback. The history of sediment infill and rates of subsidence in intramontane basins (Figs. 6  
622 and 7) combined with the analyses of fault slip data (Fig. 8), and structural data offshore (Fig. 13), confirm that brittle  
623 extension oriented from N20°E to EW occurred during an interval spanning from the Serravallian-early Tortonian to  
624 the late Tortonian (14-8 Ma) (Fig. 18). This extension is found associated with both normal and strike-slip regimes.  
625 Field tectonic data reveal that N20°E extension is more represented in HOB while the ENE-WSW to EW extension is  
626 found related with the evolution of the Almanzora fault zone, Alpujarras fault zone and Tabernas basin flanking the  
627 metamorphic domes (Table S1). There are additional evidence that EW-directed dextral strike-slip faulting occurred  
628 during the Tortonian to the South and West of the HOB. These large-scale transfer fault zones positioned on the slab  
629 edge accommodate the differential westward extension that are later cut by Tortonian NW-SE faults. These second  
630 set of faults is also observed in the magmatic crust of the EAB offshore but seismic data indicate they are Serravallian-  
631 Tortonian in age and therefore older than those identified onshore. We suggest that NW-SE normal faulting could  
632 have initiated in the EAB then migrated towards the necking domain, as slab retreat progressed and the width of the  
633 region affected by crustal thinning widened (Fig. 18). Subsidence during the Serravallian-Tortonian appears to have  
634 been lower in the EAB compared to intramontane basins onshore. This suggests that the isostatic effect of crustal  
635 thinning was compensated by a thermal anomaly in the mantle, heralding the Ca-K magmatism at 11-7 Ma (Duggen  
636 et al., 2004, 2008).

Deleted: ,

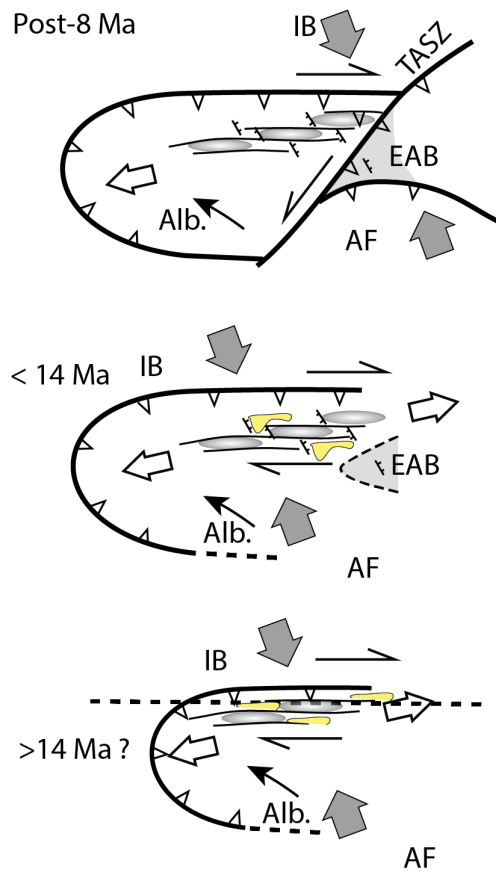
Deleted: ,

Deleted: , which was dominated by transfer faulting,

Deleted: was also

Deleted: magmatic crust of the

Deleted: suggest



644

645 **Figure 18:** Tectonic model of the evolution of the northern margin of the Alboran Rift. Large grey and white double  
 646 arrows depict shortening, which is parallel to the AF/IB convergence, and the highly oblique extension, respectively.  
 647 The thin black arrows show the motion of Alboran relative to Iberia (IB) taken from Figure 4. Half arrows depict  
 648 distributed strike-slip faulting in the Betics. NW-SE directed normal fault and strike-slip basins (yellow) are  
 649 consistent with the oblique extension. Grey-shaded ellipses represent the metamorphic domes. TASZ : simplified  
 650 representation of the Trans-Alboran Shear Zone. We also indicated EAB which mostly formed ca. 9 Ma (Duggen et  
 651 al., 2004; Booth-Rea et al., 2018).  
 652

653 Several key tectonic features found in the eastern Betics are predicted by 3D models of oblique extension (**Figure 3**).

654 They include E-W trending normal faults that are prevalent on the upper neck domain (i.e. Sierra de las Estancias and

655 HOB), and E-W strike-slip faults (Almanzora and Alpujarras fault zones). NW-SE normal faults are associated with

656 more distal domains on the continental margin where crustal thinning is the highest offshore, south of Nijar basin, and  
657 in the EAB.

658 Tectonic inversion seems, in contrast, to have been increasingly more important when approaching the Carboneras  
659 and Palomares strike-slip faults in the East since the late Tortonian.

660 Ductile thinning associated with the formation of metamorphic domes and exhumation of HP rocks is dated to 23 to  
661 16 Ma (Platt et al., 2003; Booth-Rea et al., 2015). This provides time constraint for the beginning of oblique extension  
662 and westward slab rollback. Deformation at the future location of the tear fault was probably initially diffuse and  
663 resulted in an immature oblique rift system in the South, combined with thrusting in the external zones to the North  
664 (Figure 18). In the Serravallian (14-13 Ma), accompanying slab steepening, localization of slab tearing, and  
665 propagation of thrusting in external zones, oblique extension spread over the whole central Betics. At this time,  
666 metamorphic domes exhumed to upper crustal levels (e.g. Vázquez et al., 2011) and recorded the transition from  
667 ductile shearing to brittle faulting (Figure 18). Brittle E-W-directed stretching and dextral transcurrent deformation  
668 formed at this time. The late/post-Tortonian times (from 10-8 Ma) marks a change in the tectonic evolution of the  
669 Betics and Alboran domain possibly related to the onset of slab detachment in the eastern Betics (van Hinsbergen et  
670 al., 2014; Do Couto et al., 2014; Mancilla et al., 2015a; Martínez-García et al., 2017; d'Acremont et al., 2020; García-  
671 Castellanos and Villaseñor, 2011; Spakman et al., 2018). This event is synchronous with the indentation by the  
672 magmatic arc crust of the EAB in the Águilas Arc (Ercilla et al., 2022), amplification of the metamorphic domes in  
673 the vicinity of the EBSZ (e.g. Alhambilla), transition from Ca-K in EAB to more alkaline magmatism in eastern Betics,  
674 and at the regional scale with exhumation in northern Iberia (Rat et al., 2022) and N-S shortening in northern Africa  
675 (Jolivet et al., 2021a) (Figure 18).

676 In this model, ductile stretching and ductile detachment associated with the development of the domes are the  
677 expression of oblique E-W extension. It provides a coherent scheme linking the formation of EW-directed basins in  
678 the brittle field associated with strike-slip faulting, and NW-SE/NNW-SSE sedimentary basins (Guadix, Baza,  
679 Alhabia) formed in transtension during the Tortonian. As such, the oblique extension is closely associated with STEP  
680 faulting required by westward slab rollback. The oblique rifting model we propose explain the formation of the  
681 metamorphic domes and intermontane basins and provides insight into crustal deformation, which is broadly  
682 consistent with the geodynamic models of slab rollback and tearing since 20 Ma that have been previously proposed  
683 for Alboran (Chertova et al., 2014; Spakman et al., 2018). In the latter models, however, the ENE-WSW extension in  
684 the central-eastern Betics is related to differential absolute motions between Iberia and the slab decoupled from Iberia  
685 by slab tearing. In our scenario, oblique extension is entirely related to westward lateral rollback. It can not be  
686 excluded, however, that the effect of mantle-derived slab dragging increased during the late extensional stage, from  
687 14-13 Ma, when slab tearing localized.

688 Mid-Miocene high-pressure metamorphism documented in the central Betics (e.g. Platt et al., 2013) was synchronous  
689 with slab steepening and subduction that was under way during oblique back-arc extension (Figure 18). The case of  
690 exhumation of high-pressure rocks in oblique convergence setting associated with near-parallel orogen extension is  
691 also documented in other active orogen like Taiwan (Conand et al., 2020).

Deleted: 2006

Deleted: Langhian-

Deleted: (~

Deleted: as

Deleted: mantle

Deleted: detached with no further westward slab retreat

Formatted: English (US)

Formatted: English (US)

Formatted

Formatted: English (US)

Deleted: regional

Deleted: cessation of extension and onset of uplift in the western Mediterranean region and Iberia (Jolivet et al., 2021a; Mouthereau et al., 2021; Rat et al., 2022). Ca-K magmatism occurred between 11 and 7 Ma and was followed, east of EBSZ, by the

Deleted: and

705 This highly oblique northern Alboran margin differs from typical transform fault margin such as those associated with  
706 the Atlantic ocean because it accommodates variations in intra-plate extensional movements, triggered by slab roll-  
707 back, not variations in spreading rates. Strike-slip faults may have originated as low-angle normal faults which were  
708 later reactivated as thrusts during margin inversion. Similar observations, including metamorphism, strike-slip  
709 faulting, high geothermal gradients and volcanism has been made in Seram, north of the Banda Arc, which represents  
710 another example of extremely thinned crust formed perpendicular to the direction of the slab rollback (Pownall et al.,  
711 2013). Such a narrow rifted margin associated with lithospheric STEP fault defines a class of oblique margin that is  
712 expected to be hardly preserved in the geological record due the transient nature of retreating subduction systems.  
713

714

715

715 **Data availability.** This study is based on data compilation. Data used in this study can be found in the appropriate  
716 references. Paleostress tensors obtained by the inversion of fault slip data are available online in the Supplement.  
717

718

718 **Supplement.** The supplement related to this article is available on-line at:

719

720 **Competing interests.** The authors declare that they have no conflict of interest.

#### 721 **Authors contribution**

722 ML and FM, conceptualize, prepared figures and tables, compiled and interpreted field structural data and wrote the  
723 paper. DC provided and interpreted the seismic lines, reviewed the text and contributed to the writing. AJ carefully  
724 examined the implementation of his numerical results and reviewed the text. EM, SC and VM, supervised and  
725 coordinate the different project tasks and reviewed the text.

#### 726 **Acknowledgments**

727 Victor Tendero Salmerón, Guillermo Booth-Rea, and an anonymous reviewers are warmly thanked for their comments  
728 that greatly improved the manuscript. The stereogram results were obtained using Win-Tensor, a software developed  
729 by Dr. Damien Delvaux, Royal Museum for Central Africa, Tervuren, Belgium (Delvaux and Sperner, 2003). The  
730 processed seismic data were interpreted using Kingdom IHS Suite© software. This research benefited from  
731 discussions and support of OROGEN project, an academic-industry research consortium between TOTAL, CNRS and  
732 BRGM.

733

734

735 **References**

- 736 Angrand, P., Mouthereau, F., 2021. Evolution of the Alpine orogenic belts in the Western Mediterranean region as  
 737 resolved by the kinematics of the Europe-Africa diffuse plate boundary. *Bsgf - Earth Sci Bulletin*.  
 738 <https://doi.org/10.1051/bsgf/2021031>
- 739 Argus, D.F., Gordon, R.G., DeMets, C., 2011. Geologically current motion of 56 plates relative to the no-net-  
 740 rotation reference frame. *Geochemistry, Geophysics, Geosystems* 12. <https://doi.org/10.1029/2011gc003751>
- 741 Augier, R., 2004. Evolution tardi-orogénique des Cordillères Betiques (Espagne) : apports d'une étude intégrée 1  
 742 vol., [II]-400 p.
- 743 Augier, R., Agard, P., Monié, P., Jolivet, L., Robin, C., Booth-Rea, G., 2005. Exhumation, doming and slab retreat in  
 744 the Betic Cordillera (SE Spain): in situ <sup>40</sup>Ar/<sup>39</sup>Ar ages and P–T–t paths for the Nevado-Filabride complex.  
 745 *Journal of Metamorphic Geology* 23, 357–381. <https://doi.org/10.1111/j.1525-1314.2005.00581.x>
- 746 Augier, R., Booth-Rea, G., Agard, P., Martínez-Martínez, J.M., Jolivet, L., Azañón, J.M., 2005a. Exhumation  
 747 constraints for the lower Nevado-Filabride Complex (Betic Cordillera, SE Spain): a Raman thermometry and  
 748 Tweeku multiequilibrium thermobarometry approach. *Bulletin de la Societe Geologique de France* 176, 403–  
 749 416. <https://doi.org/10.2113/176.5.403>
- 750 Augier, R., Jolivet, L., Couto, D.D., Negro, F., 2013. From ductile to brittle, late- to post-orogenic evolution of the  
 751 Betic Cordillera: Structural insights from the northeastern Internal zones. *Bulletin De La Société Géologique De*  
 752 *France* 184, 405–425. <https://doi.org/10.2113/gssgfbull.184.4-5.405>
- 753 Augier, R., Jolivet, L., Robin, C., 2005b. Late Orogenic doming in the eastern Betic Cordilleras: Final exhumation  
 754 of the Nevado-Filabride complex and its relation to basin genesis. *Tectonics* 24, n/a-n/a.  
 755 <https://doi.org/10.1029/2004tc001687>
- 756 Badji, R., Charvis, P., Bracene, R., Galve, A., Badsí, M., Ribodetti, A., Benaissa, Z., Klingelhofer, F., Medaouri,  
 757 M., Beslier, M.-O., 2014. Geophysical evidence for a transform margin offshore Western Algeria: a witness of a  
 758 subduction-transform edge propagator? *Geophys J Int* 200, 1029–1045. <https://doi.org/10.1093/gji/ggu454>
- 759 [Barcos, L., Balanyá, J.C., Díaz-Azpiroz, M., Expósito, I., Jiménez-Bonilla, A., 2015. Kinematics of the Torcal Shear  
 760 Zone: Transpressional tectonics in a salient-recess transition at the northern Gibraltar Arc. \*Tectonophysics\* 663,  
 761 62–77. <https://doi.org/10.1016/j.tecto.2015.05.002>](https://doi.org/10.1016/j.tecto.2015.05.002)
- 762 Baudouy, L., Houghton, P.D.W., Walsh, J.J., 2021. Evolution of a Fault-Controlled, Deep-Water Sub-Basin,  
 763 Tabernas, SE Spain. *Frontiers Earth Sci* 9, 767286. <https://doi.org/10.3389/feart.2021.767286>
- 764 Bessièrre, E., Jolivet, L., Augier, R., Scaillet, S., Précigout, J., Azañón, J.-M., Crespo-Blanc, A., Masini, E., Couto,  
 765 D.D., 2021. Lateral variations of pressure-temperature evolution in non-cylindrical orogens and 3-D subduction  
 766 dynamics: the Betic-Rif Cordillera example. *Bsgf - Earth Sci Bulletin*. <https://doi.org/10.1051/bsgf/2021007>
- 767 Bezada, M.J., Humphreys, E.D., Toomey, D.R., Harnafí, M., Dávila, J.M., Gallart, J., 2013. Evidence for slab  
 768 rollback in westernmost Mediterranean from improved upper mantle imaging. *Earth and Planetary Science*  
 769 *Letters* 368, 51–60. <https://doi.org/10.1016/j.epsl.2013.02.024>
- 770 Booth-Rea, G., Martínez-Martínez, J.M., Giacomini, F., 2015. Continental subduction, intracrustal shortening, and  
 771 coeval upper-crustal extension: P-T evolution of subducted south Iberian paleomargin metapelites (Betics, SE  
 772 Spain). *Tectonophysics* 663, 122–139. <https://doi.org/10.1016/j.tecto.2015.08.036>
- 773 Booth-Rea, G., Ranero, C.R., Grevemeyer, I., 2018. The Alboran volcanic-arc modulated the Messinian faunal  
 774 exchange and salinity crisis. *Scientific reports* 8, 13015. <https://doi.org/10.1038/s41598-018-31307-7>
- 775 Booth-Rea, G., Ranero, C.R., Martínez-Martínez, J.M., Grevemeyer, I., 2007. Crustal types and Tertiary tectonic  
 776 evolution of the Alborán sea, western Mediterranean. *Geochemistry, Geophysics, Geosystems* 8, n/a-n/a.  
 777 <https://doi.org/10.1029/2007gc001639>
- 778 Booth-Rea, G., Azañón, J.-M., Azor, A., García-Dueñas, V., 2004a. Influence of strike-slip fault segmentation on  
 779 drainage evolution and topography. A case study: the Palomares Fault Zone (southeastern Betics, Spain). *J*  
 780 *Struct Geol* 26, 1615–1632. <https://doi.org/10.1016/j.jsg.2004.01.007>
- 781 [Booth-Rea, G., Azañón, J.M., García-Dueñas, V., 2004b. Extensional tectonics in the northeastern Betics \(SE  
 782 Spain\): case study of extension in a multilayered upper crust with contrasting rheologies. \*Journal of structural  
 783 geology\* 26, 2039–2058. <https://doi.org/10.1016/j.jsg.2004.04.005>](https://doi.org/10.1016/j.jsg.2004.04.005)
- 784 Borque, M.J., Alzola, A.S., Martín-Rojas, I., Alfaro, P., Molina, S., Cintas, S.R., Caderot, G.R., Lacy, C., Avilés,  
 785 M., Olmo, A.H., Tortosa, F.J.G., Estévez, A., Gil, A.J., 2019. How Much Nubia-Eurasia Convergence Is  
 786 Accommodated by the NE End of the Eastern Betic Shear Zone (SE Spain)? Constraints From GPS Velocities.  
 787 *Tectonics* 38, 271–1839. <https://doi.org/10.1029/2018tc004970>
- 788 Braga, J.C., Martín, J.M., Quesada, C., 2003. Patterns and average rates of late Neogene–Recent uplift of the Betic  
 789 Cordillera, SE Spain. *Geomorphology* 50, 3–26. [https://doi.org/10.1016/s0169-555x\(02\)00205-2](https://doi.org/10.1016/s0169-555x(02)00205-2)

Formatted: Hyperlink, Font: 12 pt, Font colour: Auto

Deleted: 2004

Deleted: <https://doi.org/10.1016/j.jsg.2004.01.007>

792 Carbonell, R., Sallares, V., Pous, J., Dañoibeitia, J.J., Queralt, P., Ledo, J.J., Dueñas, V.G., 1998. A multidisciplinary  
793 geophysical study in the Betic chain (southern Iberia Peninsula). *Tectonophysics* 288, 137–152.  
794 [https://doi.org/10.1016/s0040-1951\(97\)00289-8](https://doi.org/10.1016/s0040-1951(97)00289-8)

795 Clark, S.J.P., Dempster, T.J., 2009. The record of tectonic denudation and erosion in an emerging orogen: an apatite  
796 fission-track study of the Sierra Nevada, southern Spain. *Journal of the Geological Society* 166, 87–100.  
797 <https://doi.org/10.1144/0016-76492008-041>

798 Comas, M. C., J. J. Dañoibeitia, J. Alvarez-Marón, and J. I. Soto (1995), Crustal reflections and structure in the  
799 Alboran Basin. Preliminary results of the ESCI-Alboran survey, *Rev. Soc. Geol. Esp.*, 8(4), 529 – 542.

800 Comas, M.C., García-Dueñas, V., Jurado, M.J., 1992. Neogene tectonic evolution of the Alboran Sea from MCS  
801 data. *Geo-mar Lett* 12, 157–164. <https://doi.org/10.1007/bf02084927>

802 Comas, M., and MARSIBAL 1-06 Scientific Party (2007). Preliminary results of Marsibal 1-06 cruise in the  
803 Alboran and western Algero-Balearic basins. *Geophys. Res. Abst.*, 9, 10871.

804 Conand, C., Mouthereau, F., Gamme, J., Lin, A.T., Lahfid, A., Daudet, M., Mesalles, L., Giletycz, S., Bonzani, M.,  
805 2020. Strain Partitioning and Exhumation in Oblique Taiwan Collision: Role of Rift Architecture and Plate  
806 Kinematics. *Tectonics* 39, e2019TC005798. <https://doi.org/10.1029/2019tc005798>

807 Crespo-Blanc, A., Comas, M., Balanyá, J.C., 2016. Clues for a Tortonian reconstruction of the Gibraltar Arc:  
808 Structural pattern, deformation diachronism and block rotations. *Tectonophysics* 683, 308–324.  
809 <https://doi.org/10.1016/j.tecto.2016.05.045>

810 d’Acremont, E., Lafosse, M., Rabaute, A., Teurquety, G., Couto, D.D., Ercilla, G., Juan, C., Lépinay, B.M.,  
811 Lafuerza, S., Galindo-Zaldivar, J., Estrada, F., Vazquez, J.T., Leroy, S., Poort, J., Ammar, A., Gorini, C., 2020.  
812 Polyphase Tectonic Evolution of Fore-Arc Basin Related to STEP Fault as Revealed by Seismic Reflection Data  
813 From the Alboran Sea (W-Mediterranean). *Tectonics* 39. <https://doi.org/10.1029/2019tc005885>

814 Dalziel, I.W.D., Lawver, L.A., Norton, I.O., Gahagan, L.M., 2013. The Scotia Arc: Genesis, Evolution, Global  
815 Significance. *Ann Rev Earth Pl Sc* 41, 767–793. <https://doi.org/10.1146/annurev-earth-050212-124155>

816 Daudet, M., Mouthereau, F., Brichau, S., Crespo-Blanc, A., Gautheron, C., Angrand, P., 2020. Tectono-  
817 Stratigraphic and Thermal Evolution of the Western Betic Flysch: Implications for the Geodynamics of South  
818 Iberian Margin and Alboran Domain. *Tectonics* 39. <https://doi.org/10.1029/2020tc006093>

819 Dewey, J.F., 1988. Extensional collapse of orogens. *Tectonics* 7, 1123–1139.  
820 <https://doi.org/10.1029/tc007i006p01123>

821 Dewey, J.F., Helman, M.L., Knott, S.D., Turco, E., Hutton, D.H.W., 1989. Kinematics of the western  
822 Mediterranean. Geological Society, London, Special Publications 45, 265–283.  
823 <https://doi.org/10.1144/gsl.sp.1989.045.01.15>

824 Diaz, J., Gallart, J., Carbonell, R., 2016. Moho topography beneath the Iberian-Western Mediterranean region  
825 mapped from controlled-source and natural seismicity surveys. *Tectonophysics* 692, 74–85.  
826 <https://doi.org/10.1016/j.tecto.2016.08.023>

827 Do Couto, D., Gumiaux, C., Augier, R., Lebreton, N., Folcher, N., Jouannic, G., Jolivet, L., Suc, J., Gorini, C., 2014.  
828 Tectonic inversion of an asymmetric graben: Insights from a combined field and gravity survey in the Sorbas  
829 basin. *Tectonics* 33, 1360–1385. <https://doi.org/10.1002/2013tc003458>

830 Duggen, S., Hoernle, K., Bogaard, P. van den, Rüpke, L., Morgan, J.P., 2003. Deep roots of the Messinian salinity  
831 crisis. *Nature* 422, 602–606. <https://doi.org/10.1038/nature01553>

832 Duggen, S., Hoernle, K., Bogaard, P. van den, Harris, C., 2004. Magmatic evolution of the Alboran region: The role  
833 of subduction in forming the western Mediterranean and causing the Messinian Salinity Crisis. *Earth Planet Sc*  
834 *Lett* 218, 91–108. [https://doi.org/10.1016/s0012-821x\(03\)00632-0](https://doi.org/10.1016/s0012-821x(03)00632-0)

835 Duggen, S., Hoernle, K., Klügel, A., Geldmacher, J., Thirlwall, M., Hauff, F., Lowry, D., Oates, N., 2008.  
836 Geochemical zonation of the Miocene Alborán Basin volcanism (westernmost Mediterranean): geodynamic  
837 implications. *Contrib Mineral Petr* 156, 577. <https://doi.org/10.1007/s00410-008-0302-4>

838 Echeverría, A., Khazaradze, G., Asensio, E., Gárate, J., Dávila, J.M., Suriñach, E., 2013. Crustal deformation in  
839 eastern Betics from CuaTeNeo GPS network. *Tectonophysics* 608, 600–612.  
840 <https://doi.org/10.1016/j.tecto.2013.08.020>

841 Ercilla, G., Galindo-Zaldivar, J., Estrada, F., Valencia, J., Juan, C., Casas, D., Alonso, B., Comas, M.C., Tendero-  
842 Salmerón, V., Casalbore, D., Azpiroz-Zabala, M., Bárcenas, P., Ceramicola, S., Chiocci, F.L., Idárraga-García,  
843 J., López-González, N., Mata, P., Palomino, D., Rodríguez-García, J.A., Teixeira, M., Nespereira, J., Vázquez,  
844 J.T., Yenes, M., 2022. Understanding the complex geomorphology of a deep sea area affected by continental  
845 tectonic indentation: The case of the Gulf of Vera (Western Mediterranean). *Geomorphology* 402, 108126.  
846 <https://doi.org/10.1016/j.geomorph.2022.108126>



847 Faccenna, C., Becker, T.W., Auer, L., Billi, A., Boschi, L., Brun, J.P., Capitanio, F.A., Funicello, F., Horváth, F.,  
848 Jolivet, L., Piromallo, C., Royden, L., Rossetti, F., Serpelloni, E., 2014. Mantle dynamics in the Mediterranean.  
849 *Rev Geophys* 52, 283–332. <https://doi.org/10.1002/2013rg000444>  
850 Fortuin, A.R., Krijgsman, W., 2003. The Messinian of the Nijar Basin (SE Spain): sedimentation, depositional  
851 environments and paleogeographic evolution. *Sediment Geol* 160, 213–242. [https://doi.org/10.1016/s0037-](https://doi.org/10.1016/s0037-0738(02)00377-9)  
852 [0738\(02\)00377-9](https://doi.org/10.1016/s0037-0738(02)00377-9)  
853 Fossen, H., Teyssier, C., Whitney, D.L., 2013. Transtensional folding. *Journal of structural geology* 56, 89–102.  
854 <https://doi.org/http://dx.doi.org/10.1016/j.jsg.2013.09.004>  
855 Fossen, H., Tikoff, B., 1998. Extended models of transpression and transtension, and application to tectonic settings.  
856 *Geological Society, London, Special Publications* 135, 15–33. <https://doi.org/10.1144/gsl.sp.1998.135.01.02>  
857 Galindo-Zaldivar, J., Gonzalez-Lodeiro, F., Jabaloy, A., 2015. Progressive extensional shear structures in a  
858 detachment contact in the Western Sierra Nevada (Betic Cordilleras, Spain). *Geodin Acta* 3, 73–85.  
859 <https://doi.org/10.1080/09853111.1989.11105175>  
860 Galindo-Zaldivar, J., Gil, A.J., Borque, M.J., González-Lodeiro, F., Jabaloy, A., Marin-Lechado, C., Ruano, P.,  
861 Galdeano, C.S. de, 2003. Active faulting in the internal zones of the central Betic Cordilleras (SE, Spain). *J*  
862 *Geodyn* 36, 239–250. [https://doi.org/10.1016/s0264-3707\(03\)00049-8](https://doi.org/10.1016/s0264-3707(03)00049-8)  
863 Gallais, F., Graindorge, D., Gutscher, M.-A., Klaeschen, D., 2013. Propagation of a lithospheric tear fault (STEP)  
864 through the western boundary of the Calabrian accretionary wedge offshore eastern Sicily (Southern Italy).  
865 *Tectonophysics* 602, 141–152. <https://doi.org/10.1016/j.tecto.2012.12.026>  
866 García-Castellanos, D., Villaseñor, A., 2012. Messinian salinity crisis regulated by competing tectonics and erosion  
867 at the Gibraltar arc. *Nature* 480, 359–363. <https://doi.org/10.1038/nature10651>  
868 García-Dueñas, V., Banda, E., Torné, M., Córdoba, D., Group, E.-B.W., 1994. A deep seismic reflection survey  
869 across the Betic Chain (southern Spain): first results. *Tectonophysics* 232, 77–89. [https://doi.org/10.1016/0040-](https://doi.org/10.1016/0040-1951(94)90077-9)  
870 [1951\(94\)90077-9](https://doi.org/10.1016/0040-1951(94)90077-9)  
871 Giaconia, F., Booth-Rea, G., Martínez-Martínez, J.M., Azañón, J.M., Pérez-Peña, J.V., Pérez-Romero, J., Villegas,  
872 I., 2012. Geomorphic evidence of active tectonics in the Sierra Alhamilla (eastern Betics, SE Spain).  
873 *Geomorphology* 145, 90–106. <https://doi.org/10.1016/j.geomorph.2011.12.043>  
874 Giaconia, F., Booth-Rea, G., Martínez-Martínez, J.M., Azañón, J.M., Pérez-Romero, J., Villegas, I., 2013. Mountain  
875 front migration and drainage captures related to fault segment linkage and growth: The Polopos transpressive  
876 fault zone (southeastern Betics, SE Spain). *J Struct Geol* 46, 76–91. <https://doi.org/10.1016/j.jsg.2012.10.005>  
877 Giaconia, F., Booth-Rea, G., Martínez-Martínez, J.M., Azañón, J.M., Storti, F., Artoni, A., 2014. Heterogeneous  
878 extension and the role of transfer faults in the development of the southeastern Betic basins (SE Spain).  
879 *Tectonics* 33, 2467–2489. <https://doi.org/10.1002/2014tc003681>  
880 ~~Giaconia, F., Booth-Rea, G., Ranero, C.R., Gràcia, E., Bartolome, R., Calahorra, A., Iacono, C.L., Vendrell,  
881 M.G., Cameselle, A.L., Costa, S., Peña, L.G. de la, Martínez-Loriente, S., Perea, H., Viñas, M., 2015.  
882 Compressional tectonic inversion of the Algero-Balearic basin: Latest Miocene to present oblique  
883 convergence at the Palomares margin (Western Mediterranean): Tectonic Inversion of Palomares Margin.  
884 *Tectonics* 34, 1516–1543. https://doi.org/10.1002/2015tc003861  
885 Gomez-Pugnaire, M.T., Fernandez-Soler, J.M., 1987. High-pressure metamorphism in metabasites from the Betic  
886 Cordilleras (S.E. Spain) and its evolution during the Alpine orogeny. *Contrib Mineral Petr* 95, 231–244.  
887 <https://doi.org/10.1007/bf00381273>  
888 Gómez de la Peña, L.G. de la, Grevemeyer, I., Kopp, H., Díaz, J., Gallart, J., Booth-Rea, G., Gràcia, E., Ranero,  
889 C.R., 2020a. The Lithospheric Structure of the Gibraltar Arc System From Wide-Angle Seismic Data. *J Geophys*  
890 *Res Solid Earth* 125. <https://doi.org/10.1029/2020jb019854>  
891 Gómez de la Peña, L.G. de la, Ranero, C.R., Gràcia, E., 2018. The Crustal Domains of the Alboran Basin (Western  
892 Mediterranean). *Tectonics* 37, 3352–3377. <https://doi.org/10.1029/2017tc004946>  
893 Gómez de la Peña, L.G. de la, Ranero, C.R., Gràcia, E., Booth-Rea, G., 2020b. The evolution of the westernmost  
894 Mediterranean basins. *Earth-sci Rev* 103445. <https://doi.org/10.1016/j.earscirev.2020.103445>  
895 Govers, R., Wortel, M.J.R., 2005. Lithosphere tearing at STEP faults: response to edges of subduction zones. *Earth*  
896 *Planet Sc Lett* 236, 505–523. <https://doi.org/10.1016/j.epsl.2005.03.022>  
897 Haq, B., Gorini, C., Baur, J., Moneron, J., & Rubino, J.-L. (2020). Deep Mediterranean's Messinian evaporite giant:  
898 How much salt? *Global and Planetary Change*, 184, 103052.  
899 [doi:https://doi.org/10.1016/j.gloplacha.2019.103052](https://doi.org/10.1016/j.gloplacha.2019.103052)  
900 Houghton, P.D.W., 2000. Evolving turbidite systems on a deforming basin floor, Tabernas, SE Spain.  
901 *Sedimentology* 47, 497–518. <https://doi.org/10.1046/j.1365-3091.2000.00293.x>~~

**Deleted:** Frasca, G., Gueydan, F., Brun, J.-P., Monié, P., 2016. Deformation mechanisms in a continental rift up to mantle exhumation. Field evidence from the western Betics, Spain. *Mar Petrol Geol* 76, 310–328. <https://doi.org/10.1016/j.marpetgeo.2016.04.020>

**Deleted:** <https://doi.org/10.1002/2014tc003681>

**Formatted**

908 Haughton, P.D.W., 1994. Deposits of deflected and ponded turbidity currents, Sorbas Basin, Southeast Spain. *J*  
909 *Sediment Res* 64, 233–246. <https://doi.org/10.1306/d4267d6b-2b26-11d7-8648000102c1865d>  
910 Heit, B., Mancilla, F. de L., Yuan, X., Morales, J., Stich, D., Martín, R., Molina-Aguilera, A., 2017. Tearing of the  
911 mantle lithosphere along the intermediate-depth seismicity zone beneath the Gibraltar Arc: The onset of  
912 lithospheric delamination. *Geophys Res Lett* 44, 4027–4035. <https://doi.org/10.1002/2017gl073358>  
913 Hinsbergen, D.J.J., Vissers, R.L.M., Spakman, W., 2014. Origin and consequences of western Mediterranean  
914 subduction, rollback, and slab segmentation. *Tectonics* 33, 393–419. <https://doi.org/10.1002/2013tc003349>  
915 Hodgson, D.M., Haughton, P.D.W., 2004. Impact of syndepositional faulting on gravity current behaviour and deep-  
916 water stratigraphy: Tabernas-Sorbas Basin, SE Spain. *Geological Soc Lond Special Publ* 222, 135–158.  
917 <https://doi.org/10.1144/gsl.sp.2004.222.01.08>  
918 Jabaloy-Sánchez, A., Talavera, C., Rodríguez-Peces, M.J., Vázquez-Vilchez, M., Evans, N.J., 2021. U-Pb  
919 geochronology of detrital and igneous zircon grains from the Águilas Arc in the Internal Betics (SE Spain):  
920 Implications for Carboniferous-Permian paleogeography of Pangea. *Gondwana Res* 90, 135–158.  
921 <https://doi.org/10.1016/j.gr.2020.10.013>  
922 Janowski, M., Loget, N., Gautheron, C., Barbarand, J., Bellahsen, N., Driessche, J.V. den, Babault, J., Meyer, B.,  
923 2017. Neogene exhumation and relief evolution in the eastern Betics (SE Spain): Insights from the Sierra de  
924 Gador. *Terra Nova* 29, 91–97. <https://doi.org/10.1111/ter.12252>  
925 Johnson, C., Harbury, N., Hurford, A.J., 1997. The role of extension in the Miocene denudation of the Nevado-  
926 Filábride Complex, Betic Cordillera (SE Spain). *Tectonics* 16, 189–204. <https://doi.org/10.1029/96tc03289>  
927 Jolivet, L., Baudin, T., Calassou, S., Chevrot, S., Ford, M., Issautier, B., Lasseur, E., Masini, E., Manatschal, G.,  
928 Mouthereau, F., Thionon, I., Vidal, O., 2021a. Geodynamic evolution of a wide plate boundary in the Western  
929 Mediterranean, near-field versus far-field interactions. *Bsgf - Earth Sci Bulletin* 192, 48.  
930 <https://doi.org/10.1051/bsgf/2021043>  
931 Jolivet, L., Faccenna, C., 2000. Mediterranean extension and the Africa-Eurasia collision. *Tectonics* 19, 1095–1106.  
932 <https://doi.org/10.1029/2000tc900018>  
933 Jolivet, L., Menant, A., Roche, V., Pourhiet, L.L., Maillard, A., Augier, R., Couto, D.D., Gorini, C., Thionon, I.,  
934 Canva, A., 2021b. Transfer zones in Mediterranean back-arc regions and tear faults. *Bsgf - Earth Sci Bulletin*  
935 192, 11. <https://doi.org/10.1051/bsgf/2021006>  
936 Jourdon, A., Kergaravat, C., Duclaux, G., Huguen, C., 2021. Looking beyond kinematics: 3D thermo-mechanical  
937 modelling reveals the dynamics of transform margins. *Solid Earth* 12, 1211–1232. <https://doi.org/10.5194/se-12-1211-2021>  
938 Juan, C., Ercilla, G., Javier Hernández-Molina, F., Estrada, F., Alonso, B., Casas, D., . . . Ammar, A. (2016).  
939 Seismic evidence of current-controlled sedimentation in the Alboran Sea during the Pliocene and Quaternary:  
940 Palaeoceanographic implications. *Marine Geology*, 378, 292-311.  
941 doi:<https://doi.org/10.1016/j.margeo.2016.01.006>  
942 Jurado, M.J., Comas, M.C., 1992. Well log interpretation and seismic character of the cenozoic sequence in the  
943 northern Alboran Sea. *Geo-Marine Letters* 12, 129–136.  
944 Kleverlaan, K., 1989. Neogene history of the Tabernas basin (SE Spain) and its Tortonian submarine fan  
945 development. *Geologie en Mijnbouw* 421–432.  
946 Kleverlaan, K., 1989. Three distinctive feeder-lobe systems within one time slice of the Tortonian Tabernas fan, SE  
947 Spain. *Sedimentology* 36, 25–45. <https://doi.org/10.1111/j.1365-3091.1989.tb00818.x>  
948 Kleverlaan, K., 1987. Gordo megabed: a possible seismite in a tortonian submarine fan, tabernas basin, province  
949 almeria, southeast spain. *Sediment Geol* 51, 165–180. [https://doi.org/10.1016/0037-0738\(87\)90047-9](https://doi.org/10.1016/0037-0738(87)90047-9)  
950 Koulali, A., Ouazar, D., Tahayt, A., King, R.W., Vernant, P., Reilinger, R.E., McClusky, S., Mourabit, T., Davila,  
951 J.M., Amraoui, N., 2011. New GPS constraints on active deformation along the Africa-Iberia plate boundary.  
952 *Earth Planet Sc Lett* 308, 211–217. <https://doi.org/10.1016/j.epsl.2011.05.048>  
953 Larouzière, F.D.D., Bolze, J., Bordet, P., Hernandez, J., Montecat, C., d'Estevou, P.O., 1988. The Betic segment of  
954 the lithospheric Trans-Alboran shear zone during the Late Miocene. *Tectonophysics* 152, 41–52.  
955 [https://doi.org/10.1016/0040-1951\(88\)90028-5](https://doi.org/10.1016/0040-1951(88)90028-5)  
956 Lonergan, L., White, N., 1997. Origin of the Betic-Rif mountain belt. *Tectonics* 16, 504–522.  
957 <https://doi.org/10.1029/96tc03937>  
958 Mancilla, F. de L., Booth-Rea, G., Stich, D., Pérez-Peña, J.V., Morales, J., Azañón, J.M., Martín, R., Giaconia, F.,  
959 2015a. Slab rupture and delamination under the Betics and Rif constrained from receiver functions.  
960 *Tectonophysics*. <https://doi.org/10.1016/j.tecto.2015.06.028>  
961

962 Mancilla, F. de L., Heit, B., Morales, J., Yuan, X., Stich, D., Molina-Aguilera, A., Azañón, J.M., Martín, R., 2018.  
963 A STEP fault in Central Betics, associated with lateral lithospheric tearing at the northern edge of the Gibraltar  
964 arc subduction system. *Earth Planet Sc Lett* 486, 32–40. <https://doi.org/10.1016/j.epsl.2018.01.008>  
965 Mancilla, F. de L., Stich, D., Morales, J., Martín, R., Díaz, J., Pazos, A., Córdoba, D., Pulgar, J.A., Ibarra, P.,  
966 Harnafi, M., Gonzalez-Lodeiro, F., 2015b. Crustal thickness and images of the lithospheric discontinuities in the  
967 Gibraltar arc and surrounding areas. *Geophysical Journal International* 203, 1804–1820.  
968 <https://doi.org/10.1093/gji/ggv390>  
969 Martín, J.M., Braga, J.C., Rivas, P., 1989. Coral successions in Upper Tortonian reefs in SE Spain. *Lethaia* 22, 271–  
970 286. <https://doi.org/10.1111/j.1502-3931.1989.tb01342.x>  
971 Martín, J.M., Braga, J.C., 1994. Messinian events in the Sorbas Basin in southeastern Spain and their implications in  
972 the recent history of the Mediterranean. *Sediment Geol* 90, 257–268. [https://doi.org/10.1016/0037-](https://doi.org/10.1016/0037-0738(94)90042-6)  
973 [0738\(94\)90042-6](https://doi.org/10.1016/0037-0738(94)90042-6)  
974 Martínez-García, P., Comas, M., Lonergan, L., Watts, A.B., 2017. From Extension to Shortening: Tectonic  
975 Inversion Distributed in Time and Space in the Alboran Sea, Western Mediterranean. *Tectonics* 36, 2777–2805.  
976 <https://doi.org/10.1002/2017tc004489>  
977 Martínez-García, P., Soto, J.I., Comas, M., 2011. Recent structures in the Alboran Ridge and Yusuf fault zones  
978 based on swath bathymetry and sub-bottom profiling: evidence of active tectonics. *Geo-mar Lett* 31, 19–36.  
979 <https://doi.org/10.1007/s00367-010-0212-0>  
980 Martínez-Martínez, J.M., Azañón, J.M., 1997. Mode of extensional tectonics in the southeastern Betics (SE Spain):  
981 Implications for the tectonic evolution of the peri-Alborán orogenic system. *Tectonics* 16, 205–225.  
982 <https://doi.org/10.1029/97tc00157>  
983 Martínez-Martínez, J.M., Booth-Rea, G., Azañón, J.M., Torcal, F., 2006. Active transfer fault zone linking a  
984 segmented extensional system (Betics, southern Spain): Insight into heterogeneous extension driven by edge  
985 delamination. *Tectonophysics* 422, 159–173. <https://doi.org/10.1016/j.tecto.2006.06.001>  
986 Martínez-Martínez, J.M., Soto, J.I., Balanya, J.C., 2002. Orthogonal folding of extensional detachments: Structure  
987 and origin of the Sierra Nevada elongated dome (Betics, SE Spain). *Tectonics* 21, 3-1-3–20.  
988 <https://doi.org/10.1029/2001tc001283>  
989 Martínez-Martínez, J.M., Soto, J.I., Balanya, J.C., 2004. Elongated domes in extended orogens: A mode of mountain  
990 uplift in the Betics (southeast Spain), in: *Special Paper 380: Gneiss Domes in Orogeny*. Geological Society of  
991 America, pp. 243–265. <https://doi.org/10.1130/0-8137-2380-9.243>  
992 Martínez-Martos, M., Galindo-Zaldívar, J., Martínez-Moreno, F.J., Calvo-Rayó, R., Galdeano, C.S. de, 2017.  
993 Superposition of tectonic structures leading elongated intramontane basin: the Alhabia basin (Internal Zones,  
994 Betic Cordillera). *Int J Earth Sci* 106, 2461–2471. <https://doi.org/10.1007/s00531-016-1442-9>  
995 Meighan, H.E., Brink, U. ten, Pulliam, J., 2013. Slab tears and intermediate-depth seismicity: slab tears and  
996 intermediate seismicity. *Geophys Res Lett* 40, 4244–4248. <https://doi.org/10.1002/grl.50830>  
997 Meijninger, B.M.L., Vissers, R.L.M., 2006. Miocene extensional basin development in the Betic Cordillera, SE  
998 Spain revealed through analysis of the Alhama de Murcia and Crevillente Faults: Miocene extensional basin  
999 development in the Betic Cordillera. *Basin Res* 18, 547–571. <https://doi.org/10.1111/j.1365-2117.2006.00308.x>  
1000 Montecat, C., D'Estevo, P.O., 1992. Geodynamics of the Eastern Betic late Neogene Basins. A Review. *Física de*  
1001 *la Tierra* 57–75.  
1002 Montecat, C., d'Estevo, P.O., 1999. The diversity of late Neogene sedimentary basins generated by wrench faulting  
1003 in the eastern Betic Cordillera, SE Spain. *J Petrol Geol* 22, 61–80. [https://doi.org/10.1111/j.1747-](https://doi.org/10.1111/j.1747-5457.1999.tb00459.x)  
1004 [5457.1999.tb00459.x](https://doi.org/10.1111/j.1747-5457.1999.tb00459.x)  
1005 Mora, M., 1993. Tectonic and sedimentary analysis of the Huercal-Overa region, South East Spain, Betic Cordillera.  
1006 University of Oxford, 300 pp.  
1007 Moragues, L., Ruano, P., Azañón, J.M., Garrido, C.J., Hidas, K., Booth-Rea, G., 2021. Two Cenozoic Extensional  
1008 Phases in Mallorca and Their Bearing on the Geodynamic Evolution of the Western Mediterranean. *Tectonics*  
1009 40. <https://doi.org/10.1029/2021tc006868>.  
1010 Mouthereau, F., Angrand, P., Jourdon, A., Ternois, S., Fillon, C., Calassou, S., Chevrot, S., Ford, M., Jolivet, L.,  
1011 Manatschal, G., Masini, E., Thion, I., Vidal, O., Baudin, T., 2021. Cenozoic mountain building and topographic  
1012 evolution in Western Europe: impact of billions of years of lithosphere evolution and plate kinematics. *Bsgf -*  
1013 *Earth Sci Bulletin* 192, 56. <https://doi.org/10.1051/bsgf/2021040>  
1014 Mouthereau, F., Filleaudeau, P., Vacherat, A., Pik, R., Lacombe, O., Fellin, M.G., Castellort, S., Christophoul, F.,  
1015 Masini, E., 2014. Placing limits to shortening evolution in the Pyrenees: Role of margin architecture and  
1016 implications for the Iberia/Europe convergence. *Tectonics* 33, 2283–2314. <https://doi.org/10.1002/2014tc003663>

Deleted: <https://doi.org/10.1029/2001tc001283>

1018 Neuharth, D., Brune, S., Glerum, A., Morley, C.K., Yuan, X., Braun, J., 2021. Flexural strike-slip basins. *Geology*.  
1019 <https://doi.org/10.1130/g49351.1>

1020 Nocquet, J.-M., 2012. Present-day kinematics of the Mediterranean: A comprehensive overview of GPS results.  
1021 *Tectonophysics* 579, 220–242. <https://doi.org/10.1016/j.tecto.2012.03.037>

1022 Okay, A.I., Tüysüz, O., Kaya, Ş., 2004. From transpression to transtension: changes in morphology and structure  
1023 around a bend on the North Anatolian Fault in the Marmara region. *Tectonophysics* 391, 259–282.  
1024 <https://doi.org/10.1016/j.tecto.2004.07.016>

1025 Palano, M., González, P.J., Fernández, J., 2015. The Diffuse Plate boundary of Nubia and Iberia in the Western  
1026 Mediterranean: Crustal deformation evidence for viscous coupling and fragmented lithosphere. *Earth and  
1027 Planetary Science Letters* 430, 439–447. <https://doi.org/10.1016/j.epsl.2015.08.040>

1028 Palano, M., González, P.J., Fernández, J., 2013. Strain and stress fields along the Gibraltar Orogenic Arc:  
1029 Constraints on active geodynamics. *Gondwana Res* 23, 1071–1088. <https://doi.org/10.1016/j.gr.2012.05.021>

1030 Palomeras, I., Thurner, S., Levander, A., Liu, K., Villaseñor, A., Carbonell, R., Harnafi, M., 2014. Finite-frequency  
1031 Rayleigh wave tomography of the western Mediterranean: Mapping its lithospheric structure. *Geochemistry,  
1032 Geophysics, Geosystems* 15, 140–160. <https://doi.org/10.1002/2013gc004861>

1033 Pedrera, A., Galindo-Zaldívar, J., Galdeano, C.S. de, López-Garrido, A.C., 2007. Fold and fault interactions during  
1034 the development of an elongated narrow basin: The Almanzora Neogene-Quaternary Corridor (SE Betic  
1035 Cordillera, Spain): FOLD AND FAULT INTERACTIONS. *Tectonics* 26, n/a-n/a.  
1036 <https://doi.org/10.1029/2007tc002138>

1037 Pedrera, A., Galindo-Zaldívar, J., Ruiz-Constán, A., Duque, C., Marín-Lechado, C., Serrano, I., 2009. Recent large  
1038 fold nucleation in the upper crust: Insight from gravity, magnetic, magnetotelluric and seismicity data (Sierra de  
1039 Los Filabres–Sierra de Las Estancias, Internal Zones, Betic Cordillera). *Tectonophysics* 463, 145–160.  
1040 <https://doi.org/10.1016/j.tecto.2008.09.037>

1041 Pedrera, A., Galindo-Zaldívar, J., Tello, A., Marín-Lechado, C., 2010. Intramontane basin development related to  
1042 contractional and extensional structure interaction at the termination of a major sinistral fault: The Huércal-  
1043 Overa Basin (Eastern Betic Cordillera). *J Geodyn* 49, 271–286. <https://doi.org/10.1016/j.jog.2010.01.008>

1044 Pickering, K.T., Hodgson, D.M., Platzman, E., Clark, J.D., Stephens, C., 2001. A New Type of Bedform Produced  
1045 by Backfilling Processes in a Submarine Channel, Late Miocene, Tabernas-Sorbas Basin, SE Spain. *J Sediment  
1046 Res* 71, 692–704. <https://doi.org/10.1306/2dc40960-0e47-11d7-8643000102c1865d>

1047 Pindell, J.L., Kennan, L., 2009. Tectonic evolution of the Gulf of Mexico, Caribbean and northern South America in  
1048 the mantle reference frame: an update. *Geological Soc Lond Special Publ* 328, 1–55.  
1049 <https://doi.org/10.1144/sp328.1>

1050 Platt, J.P., Behr, W.M., Johannesen, K., Williams, J.R., 2013. The Betic-Rif Arc and Its Orogenic Hinterland: A  
1051 Review. *Annual Review of Earth and Planetary Sciences* 41, 313–357. <https://doi.org/10.1146/annurev-earth-050212-123951>

1052

1053 Platt, J.P., Kelley, S.P., Carter, A., Orozco, M., 2005. Timing of tectonic events in the Alpujárride Complex, Betic  
1054 Cordillera, southern Spain. *J Geol Soc London* 162, 451–462. <https://doi.org/10.1144/0016-764903-039>

1055 Platt, J.P., Whitehouse, M.J., Kelley, S.P., Carter, A., Hollick, L., 2003. Simultaneous extensional exhumation  
1056 across the Alboran Basin: Implications for the causes of late orogenic extension. *Geology* 31, 251–254.  
1057 [https://doi.org/10.1130/0091-7613\(2003\)031<0251:seeata>2.0.co;2](https://doi.org/10.1130/0091-7613(2003)031<0251:seeata>2.0.co;2)

1058 Platt, J.P., Anczkiewicz, R., Soto, J.-I., Kelley, S.P., Thirlwall, M., 2006. Early Miocene continental subduction and  
1059 rapid exhumation in the western Mediterranean. *Geology* 34, 981–984. <https://doi.org/10.1130/g22801a.1>

1060 Platt, J.P., Vissers, R.L.M., 1989. Extensional collapse of thickened continental lithosphere: A working hypothesis  
1061 for the Alboran Sea and Gibraltar arc. *Geology* 17, 540–543. [https://doi.org/10.1130/0091-7613\(1989\)017<0540:ecotcl>2.3.co;2](https://doi.org/10.1130/0091-7613(1989)017<0540:ecotcl>2.3.co;2)

1062

1063 Platt, J.P., Whitehouse, M.J., 1999. Early Miocene high-temperature metamorphism and rapid exhumation in the  
1064 Betic Cordillera (Spain): evidence from U–Pb zircon ages. *Earth and Planetary Science Letters* 171, 591–605.

1065 Platzman, E.S., 1992. Paleomagnetic rotations and the kinematics of the Gibraltar arc. *Geology* 20, 311–314.  
1066 [https://doi.org/10.1130/0091-7613\(1992\)020<0311:pratko>2.3.co;2](https://doi.org/10.1130/0091-7613(1992)020<0311:pratko>2.3.co;2)

1067 Poisson, A., Guezou, J.C., Ozturk, A., Inan, S., Temiz, H., Gürsöy, H., Kavak, K.S., ÖZDEN, S., 1996. Tectonic  
1068 Setting and Evolution of the Sivas Basin, Central Anatolia, Turkey. *International Geology Review* 38, 838–853.  
1069 <https://doi.org/10.1080/00206819709465366>

1070 Poisson, A.M., Morel, J.L., Andrieux, J., Coulon, M., Wernli, R., Guernet, C., 1999. The origin and development of  
1071 neogene basins in the SE Betic Cordillera (SE Spain): a case study of the Tabernas-Sorbas and Huercal Overa  
1072 basins. *J Petrol Geol* 22, 97–114. <https://doi.org/10.1111/j.1747-5457.1999.tb00461.x>

Formatted: Hyperlink, Font: 12 pt, Font colour: Auto

1073 Pourhiet, L.L., Huet, B., May, D.A., Labrousse, L., Jolivet, L., 2012. Kinematic interpretation of the 3D shapes of  
1074 metamorphic core complexes: 3D SHAPES OF MCCs. *Geochem Geophys Geosystems* 13.  
1075 <https://doi.org/10.1029/2012gc004271>  
1076 Pownall, J.M., Hall, R., Watkinson, I.M., 2013. Extreme extension across Seram and Ambon, eastern Indonesia:  
1077 evidence for Banda slab rollback. *Solid Earth* 4, 277–314. <https://doi.org/10.5194/se-4-277-2013>  
1078 Rat, J., Mouthereau, F., Bricchau, S., Crémades, A., Bernet, M., Balvay, M., Ganne, J., Lahfid, A., Gautheron, C.,  
1079 2019. Tectonothermal Evolution of the Cameros Basin: Implications for Tectonics of North Iberia. *Tectonics* 38,  
1080 440–469. <https://doi.org/10.1029/2018tc005294>  
1081 Rat, J., Mouthereau, F., Bricchau, S., Vacherat, A., Fillon, C., Gautheron, C., 2022. Timing and distribution of  
1082 exhumation in the Ebro basin reveal a plate-scale 10 Ma geodynamic event. *Global Planet Change* 103973.  
1083 <https://doi.org/10.1016/j.gloplacha.2022.103973>  
1084 Reicherter, K., Hübscher, C., 2006. Evidence for a seafloor rupture of the Carboneras Fault Zone (southern Spain):  
1085 Relation to the 1522 Almería earthquake? *J Seismol* 11, 15–26. <https://doi.org/10.1007/s10950-006-9024-0>  
1086 Reinhardt, L.J., Dempster, T.J., Shroder, J.F., Persano, C., 2007. Tectonic denudation and topographic development  
1087 in the Spanish Sierra Nevada. *Tectonics* 26, n/a–n/a. <https://doi.org/10.1029/2006tc001954>  
1088 Richards, J.P., 2009. Postsubduction porphyry Cu–Au and epithermal Au deposits: Products of remelting of  
1089 subduction-modified lithosphere. *Geology* 37, 247–250. <https://doi.org/10.1130/g25451a.1>  
1090 Riding, R., Braga, J.C., Martín, J.M., Sánchez-Almazo, I.M., 1998. Mediterranean Messinian Salinity Crisis:  
1091 constraints from a coeval marginal basin, Sorbas, southeastern Spain. *Mar Geol* 146, 1–20.  
1092 [https://doi.org/10.1016/s0025-3227\(97\)00136-9](https://doi.org/10.1016/s0025-3227(97)00136-9)  
1093 Rodríguez-Fernández, J., Azor, A., Azañón, J.M., 2012. Tectonics of Sedimentary Basins 461–479.  
1094 <https://doi.org/10.1002/9781444347166.ch23>  
1095 Romagny, A., Jolivet, L., Menant, A., Bessière, E., Maillard, A., Canva, A., Gorini, C., Augier, R., 2020. Detailed  
1096 tectonic reconstructions of the Western Mediterranean region for the last 35 Ma, insights on driving  
1097 mechanisms. *Bsgf - Earth Sci Bulletin* 191, 37. <https://doi.org/10.1051/bsgf/2020040>  
1098 Rosenbaum, G., Lister, G.S., Duboz, C., 2002. Relative motions of Africa, Iberia and Europe during Alpine  
1099 orogeny. *Tectonophysics* 359, 117–129. [https://doi.org/10.1016/s0040-1951\(02\)00442-0](https://doi.org/10.1016/s0040-1951(02)00442-0)  
1100 Sanz de Galdeano, C.S., Vera, J.A., 1992. Stratigraphic record and palaeogeographical context of the Neogene  
1101 basins in the Betic Cordillera, Spain. *Basin Res* 4, 21–36. <https://doi.org/10.1111/j.1365-2117.1992.tb00040.x>  
1102 Sanz de Galdeano, C.S.D., Rodríguez-Fernández, J., López-Garrido, A.C., 1985. A strike-slip fault corridor within  
1103 the Alpujarra Mountains (Betic Cordilleras, Spain). *Geol Rundsch* 74, 641–655.  
1104 <https://doi.org/10.1007/bf01821218>  
1105 Sanz de Galdeano, C.S. de, Alfaro, P., 2004. Tectonic significance of the present relief of the Betic Cordillera.  
1106 *Geomorphology* 63, 175–190. <https://doi.org/10.1016/j.geomorph.2004.04.002>  
1107 Scotney, P., Burgess, R., Rutter, E.H., 2000. <sup>40</sup>Ar/<sup>39</sup>Ar age of the Cabo de Gata volcanic series and displacements  
1108 on the Carboneras fault zone, SE Spain. *J Geol Soc London* 157, 1003–1008.  
1109 <https://doi.org/10.1144/jgs.157.5.1003>  
1110 Sossou, M., Morrillon, A.-C., Bourgeois, J., Féraud, G., Poupeau, G., Saint-Marc, P., 1998. Late exhumation stages  
1111 of the Alpujarride Complex (western Betic Cordilleras, Spain): new thermochronological and structural data on  
1112 Los Reales and Ojen nappes. *Tectonophysics* 285, 253–273. [https://doi.org/10.1016/s0040-1951\(97\)00274-6](https://doi.org/10.1016/s0040-1951(97)00274-6)  
1113 Spakman, W., Wortel, R., 2004. The TRANSMED Atlas. The Mediterranean Region from Crust to Mantle 31–52.  
1114 [https://doi.org/10.1007/978-3-642-18919-7\\_2](https://doi.org/10.1007/978-3-642-18919-7_2)  
1115 Spakman, W., Chertova, M.V., Berg, A. van Hinsbergen, D.J.J., 2018. Puzzling features of western Mediterranean  
1116 tectonics explained by slab dragging. *Nat Geosci* 11. <https://doi.org/10.1038/s41561-018-0066-z>  
1117 Stich, D., Serpelloni, E., Mancilla, F. de L., Morales, J., 2006. Kinematics of the Iberia–Maghreb plate contact from  
1118 seismic moment tensors and GPS observations. *Tectonophysics* 426, 295–317.  
1119 <https://doi.org/10.1016/j.tecto.2006.08.004>  
1120 <https://doi.org/10.1016/j.tecto.2006.08.004>  
1121 <https://doi.org/10.1016/j.tecto.2006.08.004>  
1122 <https://doi.org/10.1016/j.tecto.2006.08.004>  
1123 <https://doi.org/10.1016/j.tecto.2006.08.004>  
1124 <https://doi.org/10.1016/j.tecto.2006.08.004>  
1125 <https://doi.org/10.1016/j.tecto.2006.08.004>  
1126 <https://doi.org/10.1016/j.tecto.2006.08.004>  
1127 <https://doi.org/10.1016/j.tecto.2006.08.004>  
1128 <https://doi.org/10.1016/j.tecto.2006.08.004>  
1129 <https://doi.org/10.1016/j.tecto.2006.08.004>  
1130 <https://doi.org/10.1016/j.tecto.2006.08.004>  
1131 <https://doi.org/10.1016/j.tecto.2006.08.004>  
1132 <https://doi.org/10.1016/j.tecto.2006.08.004>  
1133 <https://doi.org/10.1016/j.tecto.2006.08.004>  
1134 <https://doi.org/10.1016/j.tecto.2006.08.004>  
1135 <https://doi.org/10.1016/j.tecto.2006.08.004>  
1136 <https://doi.org/10.1016/j.tecto.2006.08.004>  
1137 <https://doi.org/10.1016/j.tecto.2006.08.004>  
1138 <https://doi.org/10.1016/j.tecto.2006.08.004>  
1139 <https://doi.org/10.1016/j.tecto.2006.08.004>  
1140 <https://doi.org/10.1016/j.tecto.2006.08.004>  
1141 <https://doi.org/10.1016/j.tecto.2006.08.004>  
1142 <https://doi.org/10.1016/j.tecto.2006.08.004>  
1143 <https://doi.org/10.1016/j.tecto.2006.08.004>  
1144 <https://doi.org/10.1016/j.tecto.2006.08.004>  
1145 <https://doi.org/10.1016/j.tecto.2006.08.004>  
1146 <https://doi.org/10.1016/j.tecto.2006.08.004>  
1147 <https://doi.org/10.1016/j.tecto.2006.08.004>  
1148 <https://doi.org/10.1016/j.tecto.2006.08.004>  
1149 <https://doi.org/10.1016/j.tecto.2006.08.004>  
1150 <https://doi.org/10.1016/j.tecto.2006.08.004>  
1151 <https://doi.org/10.1016/j.tecto.2006.08.004>  
1152 <https://doi.org/10.1016/j.tecto.2006.08.004>  
1153 <https://doi.org/10.1016/j.tecto.2006.08.004>  
1154 <https://doi.org/10.1016/j.tecto.2006.08.004>  
1155 <https://doi.org/10.1016/j.tecto.2006.08.004>  
1156 <https://doi.org/10.1016/j.tecto.2006.08.004>  
1157 <https://doi.org/10.1016/j.tecto.2006.08.004>  
1158 <https://doi.org/10.1016/j.tecto.2006.08.004>  
1159 <https://doi.org/10.1016/j.tecto.2006.08.004>  
1160 <https://doi.org/10.1016/j.tecto.2006.08.004>  
1161 <https://doi.org/10.1016/j.tecto.2006.08.004>  
1162 <https://doi.org/10.1016/j.tecto.2006.08.004>  
1163 <https://doi.org/10.1016/j.tecto.2006.08.004>  
1164 <https://doi.org/10.1016/j.tecto.2006.08.004>  
1165 <https://doi.org/10.1016/j.tecto.2006.08.004>  
1166 <https://doi.org/10.1016/j.tecto.2006.08.004>  
1167 <https://doi.org/10.1016/j.tecto.2006.08.004>  
1168 <https://doi.org/10.1016/j.tecto.2006.08.004>  
1169 <https://doi.org/10.1016/j.tecto.2006.08.004>  
1170 <https://doi.org/10.1016/j.tecto.2006.08.004>  
1171 <https://doi.org/10.1016/j.tecto.2006.08.004>  
1172 <https://doi.org/10.1016/j.tecto.2006.08.004>  
1173 <https://doi.org/10.1016/j.tecto.2006.08.004>  
1174 <https://doi.org/10.1016/j.tecto.2006.08.004>  
1175 <https://doi.org/10.1016/j.tecto.2006.08.004>  
1176 <https://doi.org/10.1016/j.tecto.2006.08.004>  
1177 <https://doi.org/10.1016/j.tecto.2006.08.004>  
1178 <https://doi.org/10.1016/j.tecto.2006.08.004>  
1179 <https://doi.org/10.1016/j.tecto.2006.08.004>  
1180 <https://doi.org/10.1016/j.tecto.2006.08.004>  
1181 <https://doi.org/10.1016/j.tecto.2006.08.004>  
1182 <https://doi.org/10.1016/j.tecto.2006.08.004>  
1183 <https://doi.org/10.1016/j.tecto.2006.08.004>  
1184 <https://doi.org/10.1016/j.tecto.2006.08.004>  
1185 <https://doi.org/10.1016/j.tecto.2006.08.004>  
1186 <https://doi.org/10.1016/j.tecto.2006.08.004>  
1187 <https://doi.org/10.1016/j.tecto.2006.08.004>  
1188 <https://doi.org/10.1016/j.tecto.2006.08.004>  
1189 <https://doi.org/10.1016/j.tecto.2006.08.004>  
1190 <https://doi.org/10.1016/j.tecto.2006.08.004>  
1191 <https://doi.org/10.1016/j.tecto.2006.08.004>  
1192 <https://doi.org/10.1016/j.tecto.2006.08.004>  
1193 <https://doi.org/10.1016/j.tecto.2006.08.004>  
1194 <https://doi.org/10.1016/j.tecto.2006.08.004>  
1195 <https://doi.org/10.1016/j.tecto.2006.08.004>  
1196 <https://doi.org/10.1016/j.tecto.2006.08.004>  
1197 <https://doi.org/10.1016/j.tecto.2006.08.004>  
1198 <https://doi.org/10.1016/j.tecto.2006.08.004>  
1199 <https://doi.org/10.1016/j.tecto.2006.08.004>  
1200 <https://doi.org/10.1016/j.tecto.2006.08.004>  
1201 <https://doi.org/10.1016/j.tecto.2006.08.004>  
1202 <https://doi.org/10.1016/j.tecto.2006.08.004>  
1203 <https://doi.org/10.1016/j.tecto.2006.08.004>  
1204 <https://doi.org/10.1016/j.tecto.2006.08.004>  
1205 <https://doi.org/10.1016/j.tecto.2006.08.004>  
1206 <https://doi.org/10.1016/j.tecto.2006.08.004>  
1207 <https://doi.org/10.1016/j.tecto.2006.08.004>  
1208 <https://doi.org/10.1016/j.tecto.2006.08.004>  
1209 <https://doi.org/10.1016/j.tecto.2006.08.004>  
1210 <https://doi.org/10.1016/j.tecto.2006.08.004>  
1211 <https://doi.org/10.1016/j.tecto.2006.08.004>  
1212 <https://doi.org/10.1016/j.tecto.2006.08.004>  
1213 <https://doi.org/10.1016/j.tecto.2006.08.004>  
1214 <https://doi.org/10.1016/j.tecto.2006.08.004>  
1215 <https://doi.org/10.1016/j.tecto.2006.08.004>  
1216 <https://doi.org/10.1016/j.tecto.2006.08.004>  
1217 <https://doi.org/10.1016/j.tecto.2006.08.004>  
1218 <https://doi.org/10.1016/j.tecto.2006.08.004>  
1219 <https://doi.org/10.1016/j.tecto.2006.08.004>  
1220 <https://doi.org/10.1016/j.tecto.2006.08.004>  
1221 <https://doi.org/10.1016/j.tecto.2006.08.004>  
1222 <https://doi.org/10.1016/j.tecto.2006.08.004>  
1223 <https://doi.org/10.1016/j.tecto.2006.08.004>  
1224 <https://doi.org/10.1016/j.tecto.2006.08.004>  
1225 <https://doi.org/10.1016/j.tecto.2006.08.004>  
1226 <https://doi.org/10.1016/j.tecto.2006.08.004>  
1227 <https://doi.org/10.1016/j.tecto.2006.08.004>  
1228 <https://doi.org/10.1016/j.tecto.2006.08.004>  
1229 <https://doi.org/10.1016/j.tecto.2006.08.004>  
1230 <https://doi.org/10.1016/j.tecto.2006.08.004>  
1231 <https://doi.org/10.1016/j.tecto.2006.08.004>  
1232 <https://doi.org/10.1016/j.tecto.2006.08.004>  
1233 <https://doi.org/10.1016/j.tecto.2006.08.004>  
1234 <https://doi.org/10.1016/j.tecto.2006.08.004>  
1235 <https://doi.org/10.1016/j.tecto.2006.08.004>  
1236 <https://doi.org/10.1016/j.tecto.2006.08.004>  
1237 <https://doi.org/10.1016/j.tecto.2006.08.004>  
1238 <https://doi.org/10.1016/j.tecto.2006.08.004>  
1239 <https://doi.org/10.1016/j.tecto.2006.08.004>  
1240 <https://doi.org/10.1016/j.tecto.2006.08.004>  
1241 <https://doi.org/10.1016/j.tecto.2006.08.004>  
1242 <https://doi.org/10.1016/j.tecto.2006.08.004>  
1243 <https://doi.org/10.1016/j.tecto.2006.08.004>  
1244 <https://doi.org/10.1016/j.tecto.2006.08.004>  
1245 <https://doi.org/10.1016/j.tecto.2006.08.004>  
1246 <https://doi.org/10.1016/j.tecto.2006.08.004>  
1247 <https://doi.org/10.1016/j.tecto.2006.08.004>  
1248 <https://doi.org/10.1016/j.tecto.2006.08.004>  
1249 <https://doi.org/10.1016/j.tecto.2006.08.004>  
1250 <https://doi.org/10.1016/j.tecto.2006.08.004>  
1251 <https://doi.org/10.1016/j.tecto.2006.08.004>  
1252 <https://doi.org/10.1016/j.tecto.2006.08.004>  
1253 <https://doi.org/10.1016/j.tecto.2006.08.004>  
1254 <https://doi.org/10.1016/j.tecto.2006.08.004>  
1255 <https://doi.org/10.1016/j.tecto.2006.08.004>  
1256 <https://doi.org/10.1016/j.tecto.2006.08.004>  
1257

1130 van Hinsbergen, D.J.J., Vissers, R.L.M., Spakman, W., 2014. Origin and consequences of western Mediterranean  
1131 subduction, rollback, and slab segmentation. *Tectonics* 33, 393–419. <https://doi.org/10.1002/2013tc003349>  
1132 Vázquez, M., Jabaloy, A., Barbero, L., Stuart, F.M., 2011. Deciphering tectonic- and erosion-driven exhumation of  
1133 the Nevado-Filábride Complex (Betic Cordillera, Southern Spain) by low temperature thermochronology:  
1134 Deciphering tectonic- and erosion-driven exhumation. *Terra Nova* 23, 257–263. <https://doi.org/10.1111/j.1365-3121.2011.01007.x>  
1135  
1136 Vergés, J., Fernández, M., 2012. Tethys–Atlantic interaction along the Iberia–Africa plate boundary: The Betic–Rif  
1137 orogenic system. *Tectonophysics* 579, 144–172. <https://doi.org/10.1016/j.tecto.2012.08.032>  
1138 Vernant, P., Fadil, A., Mourabit, T., Ouazar, D., Koulali, A., Davila, J.M., Garate, J., McClusky, S., Reilinger, R.,  
1139 2010. Geodetic constraints on active tectonics of the Western Mediterranean: Implications for the kinematics and  
1140 dynamics of the Nubia-Eurasia plate boundary zone. *J Geodyn* 49, 123–129.  
1141 <https://doi.org/10.1016/j.jog.2009.10.007>  
1142 Villasenor, A., Chevrot, S., Harnafi, M., Gallart, J., Pazos, A., Serrano, I., Córdoba, D., Pulgar, J.A., Ibarra, P.,  
1143 2015. Subduction and volcanism in the Iberia–North Africa collision zone from tomographic images of the  
1144 upper mantle. *Tectonophysics*. <https://doi.org/10.1016/j.tecto.2015.08.042>  
1145 Waldner, M., Bellahsen, N., Mouthereau, F., Bernet, M., Pik, R., Rosenberg, C.L., Balvay, M., 2021. Central  
1146 Pyrenees Mountain Building: Constraints From New LT Thermochronological Data From the Axial Zone.  
1147 *Tectonics* 40. <https://doi.org/10.1029/2020tc006614>  
1148 Weijermars, R., Roep, Th.B., Eeckhout, B.V. den, Postma, G., Kleverlaan, K., 1985. Uplift history of a Betic fold  
1149 nappe inferred from Neogene–Quaternary sedimentation and tectonics (in the Sierra Alhamilla and Almería,  
1150 Sorbas and Tabernas Basins of the Betic Cordilleras, SE Spain). *Geologie en Mijnbouw* 397–411.  
1151 Zeck, H.P., Monié, P., Villa, I.M., Hansen, B.T., 1992. Very high rates of cooling and uplift in the Alpine belt of the  
1152 Betic Cordilleras, southern Spain. *Geology* 20, 79. [https://doi.org/10.1130/0091-7613\(1992\)020<0079:vhroca>2.3.co;2](https://doi.org/10.1130/0091-7613(1992)020<0079:vhroca>2.3.co;2)  
1153  
1154